

SYNTHESIS OF A STATE MODEL
FOR HYSTERETIC DEVICES

Thesis for the Degree of Ph. D.
MICHIGAN STATE UNIVERSITY
ARTICE M. DAVIS
1972

LIBRARY
Michigan State
University

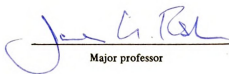
This is to certify that the
thesis entitled
SYNTHESIS OF A STATE MODEL
FOR HYSTERETIC DEVICES

presented by

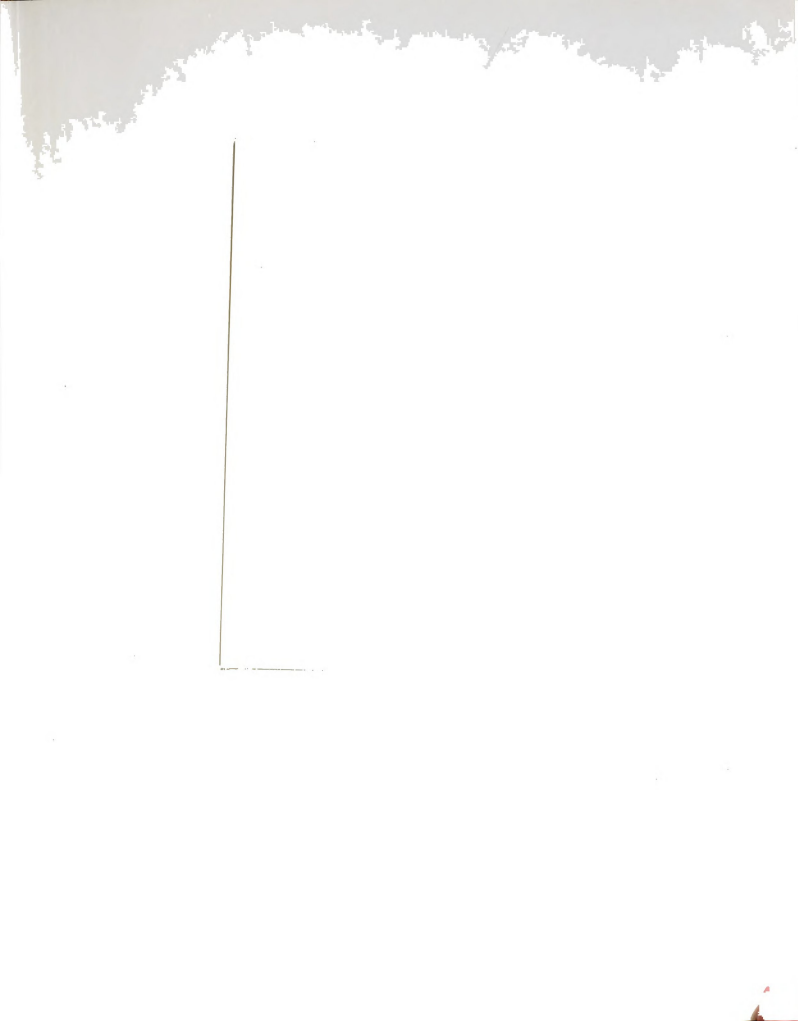
Artice M. Davis

has been accepted towards fulfillment
of the requirements for

Ph. D. degree in SYS


Major professor

Date 8/14/72











ABSTRACT

SYNTHESIS OF A STATE MODEL FOR HYSTERETIC DEVICES

By

Artice M. Davis

In its most general setting, the fundamental task which this thesis attempts to accomplish is an investigation of the application of a specific model to the characterization of hysteretic effects. More specifically, an algorithm is outlined for the synthesis of the model parameters from experimental measurements on an actual hysteretic device.

In the course of development, a discrete state space representation is derived for the model. A simulation routine using this state description is then outlined. A more general continuous model is developed, and a state space description for it is advanced. Another simulation algorithm--in this case a continuous one--is presented.

As a consequence of the work embodied here, a computer package is available for modeling hysteretic devices and for incorporating them into larger networks for simulation purposes.

SYNTHESIS OF A STATE MODEL
FOR HYSTERETIC DEVICES

By

Artice M. Davis

A THESIS

Submitted to
Michigan State University
in partial fulfillment of the requirements
for the degree of

DOCTOR OF PHILOSOPHY

Department of Electrical Engineering and Systems Science

1972

G78872

To Boojum

ACKNOWLEDGMENTS

It has been said that imitation is the sincerest form of flattery. If this be so then, in a sense, this thesis could be construed as a compliment to Dr. J. A. Resh. An attempt has certainly been made to assume a particular mental posture characteristic of Dr. Resh: an attitude which I term resilience of research. I am thankful to Dr. R. O. Barr, not only for his contribution to the current work, but also for valuable guidance during work prior to this. The other members of my committee, Dr. J. S. Frame, Dr. J. B. Kreer, and Dr. P. D. Fisher, provided occasional sorely needed injections of enthusiasm. A special word of appreciation is extended to my wife, Lalah. Indeed, if degrees were jointly held, half of this one would justly belong to her.

TABLE OF CONTENTS

	Page
ABSTRACT	
ACKNOWLEDGMENTS	ii
I. INTRODUCTION	1
1.1 The Problem	1
1.2 Background	4
II. THE BEAM-ROD ANALOGY	13
2.1 The Basic Model	13
2.2 The Resh-Preisach Plane	16
2.3 Mathematical Development	18
2.4 The Process Model	22
2.5 Preliminary Results and Characteristics	25
III. SYNTHESIS OF THE MODEL	30
3.1 The Definition of the Problem	30
3.2 Experimental Measurements	33
3.3 The Search for the Support of the Distribution Function	36
3.4 Synthesis Considerations	59
3.5 Synthesis of the Distribution Functions	63
IV. THE CONTINUOUS STATE MODEL	80
4.1 The Need for a Continuous Model	80
4.2 The Continuous State Representation	80
4.3 The Continuous Simulation Algorithm	86
V. CONCLUSIONS	95
REFERENCES	98
APPENDIX. THE PRACTICAL ASPECTS OF INTEGRATION	100

CHAPTER I

INTRODUCTION

The phenomenon of hysteresis arises in a multiplicity of situations in the physical realm. In such diverse fields as physiology, elasticity, electrical engineering and soil science¹⁻⁴, hysteresis effects appear--and astonishingly exhibit the same class of characteristics. This uniformity is a good prognostication for an attempted generalization of a specific model to encompass a wider category. In the work presented here, the immediate tie is to the properties of ferromagnetic material. An underlying current of thought, however, tends toward hypothesizing that the characteristics of this particular process proffer a basis for the representation of more general types of hysteretic phenomena.

1.1. The Problem

In most works purporting an explanation of hysteresis effects, one fact is conspicuous in its absence: the definition of the term itself. Some of the notable features of ferromagnetic material--the shape of the saturation loop, minor loop behavior, and cyclic demagnetization--are usually listed, but no attempt is made at a general definition. Thus, it is perhaps of benefit to attempt such a clarification at this point.

The principle feature which distinguishes ferromagnetism, mechanical backlash, and the like from other effects is their static nature. Although rate dependent effects are present, they only

appear as perturbations to the static characteristics. The attempt here will be the clarification of the essential elements of hysteresis-- those present at extremely low rates of variation. The following definition could be phrased in terms of relations between pairs of variables associated with a multiterminal component or system, but it will be tacit here that the object under consideration is two-terminal.

Consider, then, the oriented object of Figure 1.1.1:

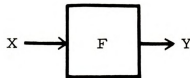


Figure 1.1.1

X and Y are input and output time functions, and F is the operator associated with the object. Let X range over the space of testing functions such as the one shown in Figure 1.1.2.

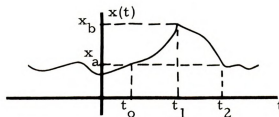


Figure 1.1.2

In order to qualify as a testing function, a given input X must possess the following property: there must exist two adjacent time intervals (t_0, t_1) and (t_1, t_2) such that X is monotone in opposite senses in the two intervals. t_0 , t_1 , and t_2 are arbitrary.

Now let x and y be the restrictions of X and Y to (t_0, t_2) , and let R_{xy} be the consequent relation in $R^X R$. Define $x(t_0) = x_a$ and $x(t_2) = x_b$, and let M be the maximum value of the magnitude of the slope of x on the interval (t_0, t_2) . Then:

Definition: If there exist a pair of values x_a and x_b such that, for each associated testing function with finite M , R_{xy} is double valued; and if for X fixed outside (t_0, t_2) R_{xy} approaches a limiting double valued relation as M goes to zero, the object will be called hysteretic.

Note that this proposed definition precludes such objects as integrators and RC circuits from being labeled hysteretic. Although double valued relations R_{xy} are produced, they are always dependent upon the exact nature of the input. The definition above characterizes objects which do not have this precise dependence.

With the definition disposed of, more practical questions begin to arise. Do all replicas of a given object behave in the same manner? If so, can their behavior be generically characterized-- does there exist a model representative of them all? How catholic is that model with regard to the larger class of hysteretic objects? Finally, one is led to ask the very practical "nuts and bolts" question: "Can the model parameters be determined by experimental measurements on the object?"

Some of these questions have been answered. Empirical observations indicate that all replicas do behave generally in like manner. Several models have been proposed, both for specific processes and for hysteresis in the abstract, although their collective merits

are moot. The question of catholicity has not been adjudicated. A model for the ferromagnetic process has recently been proposed⁵, and this thesis attempts to answer the synthesis question for it. In addition, certain features of the model are developed farther-- features such as its state-space representation and simulation characteristics.

1.2. Background

The phenomenon of ferromagnetic hysteresis is usually treated by simply ignoring its existence. When it is not ignored, the procedure is almost always one involving piecewise linearization of the major loops. Although the area of circuit analysis has been under development since the very beginnings of electrical engineering, there is yet a paucity of theory pertaining to iron core inductors. Several interesting assaults have been launched against the bastion of the problem, but on the whole there has been a dearth of "doings" in the area. In fact, the different approaches can be discussed serially. These different methods are effectively enumerated by tagging them with names: Ewing, Weiss, Preisach, Volterra, Chua, and Resh. The first five will be synopsized in this section, and the sequel will be concerned with a full development of the last.

Ewing's Model⁶. Ewing's work adumbrated that of Weiss and a number of others. His main contribution consisted of the development of a physical analogy to the behavior of a ferromagnet. As indicated in Figure 1.2.1, his model consists of a number of small magnetic dipoles, pivoted and free to rotate in a plane.

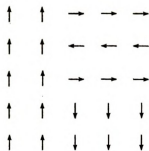


Figure 1.2.1

In the absence of any external field, their mutual interaction aligns them in such fashion that the potential energy of the configuration is a minimum. Such a configuration is not necessarily unique--one such is illustrated in Figure 1.2.1.

If an external field is now applied in some arbitrary direction, the dipoles begin to rotate in an elastic fashion about their axes. The term elastic is used in the sense that should the field be reduced, the rotation will exactly reverse. At some critical value of applied field, the assemblage becomes unstable, and an abrupt macroscopic change in configuration results. The change is, as intuitively expected, nonreversible. This particular happenstance is the result of the interaction of the dipoles, and is in such a manner as to reduce the total energy of the configuration.

As the applied field continues to increase, there will be a further elastic rotation of the dipoles and other irreversible changes of configuration. A final elastic rotation evinces itself as saturation is approached. If the external field is now reduced, the initial path will not be retraversed by consequence of the previous irreversible changes. The resulting hysteresis loop looks remarkably similar to that observed for iron. The Ewing model results are depicted in Figure 1.2.2.

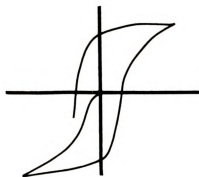


Figure 1.2.2

As a physical experiment, Ewing's model is simple--the mathematics is more complex. Several investigators⁷ have attempted the analysis of Ewing models in one, two and three dimensions. All tries proved fruitless for models whose number of component dipoles was other than trivially small. Another seeming disadvantage of the model is that when scaled to atomic dimensions it gives quantitatively incorrect results⁷. This is perhaps not such an important objection for, as one writer has pointed out⁸, the physical processes involved bear such close resemblance to those now known to hold for ferromagnetic action. The model remains valid as an analogy, albeit a mathematically intractable one.

Weiss' Work⁹. Weiss' analysis was an attempt to describe the Ewing model in mathematical terms. As a prelude, Langevin¹⁰ had derived an expression for the magnetization of a paramagnetic material--one consisting of magnetic dipoles having no interaction, but which are under the influence of thermal effects. The Ewing model, as mentioned above, is intractable. This complexity led Weiss to postulate as an approximation that each dipole experiences a total magnetic field made up of the external field and an additive component due to the effects of the other dipoles. This additive

component became known as the "molecular field". Weiss made the assumption that it is proportional to, and collinear with, the total magnetization. Combining this with Langevin's previous results, he arrived at an expression for the magnetization as a function of applied field.

Space here does not permit replication of the works of Langevin and Weiss, but the important features can be underscored. This attack led to the first analytical expression for ferromagnetic behavior. It permitted calculation of thermal effects and led to the postulation of ferromagnetic domains. On the other hand, there were serious flaws. The assumption that the molecular field is collinear with the magnetization vector is too restrictive, and he allowed for no dependence on the crystalline structure of the material.

Volterra's Theory¹¹. With Volterra there was an effective shift of emphasis; he attempted to explain hysteretic action as a general phenomenon. Although Volterra seems to have been motivated primarily by the elastic behavior of solids, he postulated the validity of his theory on a more sweeping plane. He considered a physical system to be an operator defined on a suitable class of functions. He further restricted himself to linear operators of the special form

$$x(t) = K y(t) + \int_{-\infty}^t \phi(t, z) y(z) dz$$

where $x(t)$ is the input function and $y(t)$ the output. For ferromagnetic material, this assumes the form

$$H(t) = \mu_0^{-1} B(t) + \int_{-\infty}^t \phi(t, z) B(z) dz$$

where the symbols have the usual significance. $\phi(t, z)$ is termed the hereditary kernel. These equations fall into the general category commonly given the name Volterra's Integral Equations of the Second Kind. The pioneering efforts of Volterra and Fredholm were directed toward solution of these equations for the output function in terms of the input.

The innate disadvantage of this theory is the absence of any correlation between the describing equation and the physical mechanisms underlying the hysteretic process. It will be demonstrated later that there is a correspondence in form with ferromagnetism, but a very ad hoc assumption continues to mar its features.

Preisach's Solution¹². After its enunciation by Preisach, this theory went through a process of evolution, culminating in the work of Biorci and Pescetti¹³. From a practical viewpoint, their work has produced quite useful results in spite of the limitations to be alluded to later. It is perhaps worthwhile to note that the resulting model bears certain points of contact with the one currently being investigated, although the latter is more general in nature.

The Preisach development begins with the assumption that the body of ferromagnetic material under consideration consists of an aggregate of infinitesimal volume elements, each characterized by the relation of Figure 1.2.3. I is the magnetization of the infinitesimal volume experiencing a field intensity H . a and b are allowed to vary from one element to another, but I_0 remains fixed. It must be true that $a \geq b$, since energy can only be dissipated in each element. In addition, no element has $a \geq H_s$ or $b \leq -H_s$, the saturation field intensity. It is possible to characterize the model by a region

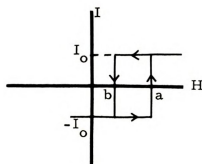


Figure 1.2.3

in the (a, b) plane, on which is defined a distribution function $\phi(a, b)$. $\phi(a, b) da db$, then, is the number of elements which possess (a, b) pairs lying in the rectangular region centered at (a, b) with sides of length da and db . The planar situation is shown in Figure 1.2.4.

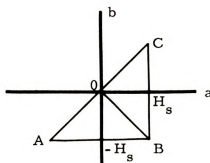


Figure 1.2.4

It has been shown that all volumes with defining number pairs (a, b) belonging to AOB go to positive magnetization under a cyclically decreasing H field. All others go to negative magnetization.

If the distribution function ϕ is known, it is possible to determine the magnetization as a function of the applied field. Any continuous input function can be broken up into monotone segments, and these monotone segments define resulting regions in the plane.

The magnetization is then expressible as

$$I(H) = 2 I_s \iint_Q \phi(a, b) da db$$

where I_s is the saturation value of I associated with H_s , and Q is that region whose elements have undergone an odd number of reversals. A procedure has been outlined for determining ϕ from experimental measurements--if certain restrictions are imposed. A more careful discussion of this theory is contained in reference 13.

The Preisach theory has been quite useful to practically oriented investigators, but there are several flaws. Primary among them is the entirely irreversible nature of the process. This is a result of the square loop characterization of the elemental volumes. It is tempting to equate these volumes with ferromagnetic domains. They do not, however, exhibit such physical properties as elastic wall growth which domains are known to possess. Thus, the model must be considered as an abstract analogy to hysteretic behavior, and its application must be limited to materials in which the irreversible processes are dominant

Chua's Method¹⁴. Chua, in the manner of Volterra, attempted to model the general phenomenon of hysteresis by mathematical abstraction. He proposed the nonlinear differential equation

$$\frac{dy}{dt} = g \left[x(t) - f(y(t)) \right]$$

for which he proceeded to demonstrate hysteretic behavior. In order that they be realizable, the functions g and f must be odd and invertible. Chua outlines a simple procedure for deriving f and g from measurements on the saturation loop. This implies that devices with identical saturation loops must exhibit identical minor loops. It

would appear from experimental observations that this is too simplistic a view.

In addition to this, the model also implies that a complete set of state variables is provided by the instantaneous values of the input and output. Experiment indicates that, at least for ferromagnetic devices, there is a major loop passing through each point (x, y) inside the saturation loop. Thus, assumption of an initial state (x, y) should immediately result in the traversal of that loop. Simulation of the Chua model does not result in such closure--see Figure 1.2.5. The solution spirals inward and asymptotically approaches a steady state loop.

Discussion of Previous Work. In all of the prior work, one fact is evident: with the exception of Chua, no investigator has approached the subject from an engineering stance. In all cases, strong features were nullified to some extent by debilitating ones. An additional factor exhibited by all these models is the characteristic of abstract analogy to physical hysteretic behavior--not necessarily a point of weakness, and one shared by the present model. The model to be considered next appears to obviate many of these shortcomings. The state characterization techniques and synthesis procedures developed for it appear to extend to some of the previous models as well.

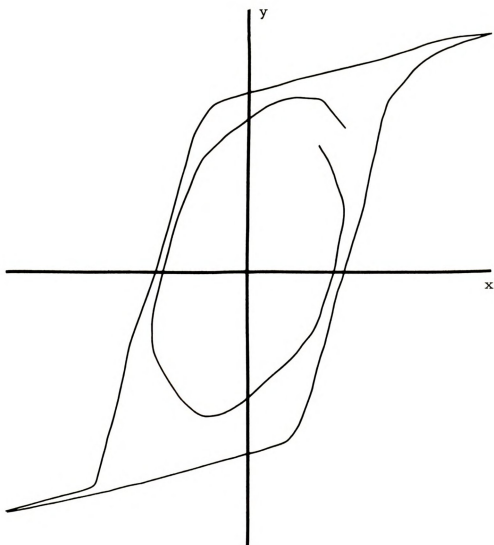


Figure 1.2.5

CHAPTER II

THE BEAM-ROD ANALOGY

As mentioned previously, all of the hysteretic models to date have possessed inherent shortcomings. They have run the gamut from the abstract to the concrete, but there has been a common thread of correspondence, in the main, among them. The disappointing feature is the lack of any sort of chronological evolution. In 1969, however, Resh⁵ delivered a paper describing a model which appears to consolidate the features of the previous models, while improving upon and generalizing their capabilities. This correspondence is a posteriori, and is deeply imbedded in the theoretical aspects of the model, but definitely exists. Hence, its more general nature can be shown. This section is devoted to the exposition of the basic model and its ancillary aspects. Following Resh's development, the basic model will be described; afterward its correspondence with the physics of ferromagnetism will be delimited. Some related conceptual and computational features will then be developed.

2.1. The Basic Model⁵

The essential feature of the model investigated here is its form as a mechanical analogy to the ferromagnetic process. Its configuration is illustrated in Figure 2.1.1. It consists of a set of flexible beams attached to a rigid surface P and a rod R which moves parallel with the surface. There are two types of beam: one variety is



Figure 2. 1. 1

engaged by the rod as it moves past the beam's equilibrium position from left to right, and the other kind is picked up as the rod moves past it from right to left. The former type of beam will be dubbed "right active" and the latter "left active". The equilibrium positions of the beams are distributed in some manner, and the drop-off positions and coefficients of elasticity are allowed to vary from one beam to another. While a given beam is engaged by the rod, its force versus flexure relation is assumed linear--the beam merely behaves like a linear spring affixed to the rod.

There are two important characteristics which should be noted at this point. The nature of the flexing process of an engaged beam is elastic and reversible until the drop-off point is attained. The other item of note is the autonomous nature of the process when the beam drop point is exceeded. This represents an energy dissipation activity which is decoupled from the input. These two features provide, on a macroscopic energy process level, a tight correspondence with solid state theory.

The current status of ferromagnetic theory is such that a qualitative description of the magnetization curve is available. In the virgin, or undisturbed, state, a body of ferromagnetic material can be thought of as consisting of elementary dipoles. These dipoles are arranged such that all dipole moments in a small volume element,

or domain, have the same direction. The boundary of each volume, called a Bloch wall, consists of a layer of atoms several atoms thick. In the Bloch wall, the magnetization varies smoothly in direction from one side to the other, with parallelism being maintained on each side with the contiguous domain magnetization.

When an external field is applied and increased from zero, whichever of two adjacent domains has its magnetization vector closest in direction to the applied field begins to engage in territorial expansion at the expense of its neighbor. The atoms in the Bloch wall begin to rotate in order to align themselves more closely with those of the burgeoning domain; hence, with the applied field. This process is, of course, being replicated thousands of times throughout the mass of material. If the applied field continues to increase, a point is eventually reached such that less energy is required to maintain the configuration if those domains which have magnetizations more-or-less antiparallel with the applied field flip those magnetizations by π radians. This activity, when initiated, proceeds autonomously, with energy being irretrievably lost by the concomitant eddy currents. All these reversals do not, of course, proceed in unison. They are, on the contrary, distributed with different critical values of field; this produces the discontinuities known as the Barkhausen effect.

As the process continues, another type of activity is initiated: gross restructuring of individual domain geometry. This is also an irreversible stage in the process. Finally, as saturation is approached, all domains rotate their magnetization vectors elastically to produce final alignment with the applied field.

The preceding discussion indicates that there are two processes at work--one reversible, the other irreversible and autonomous when initiated. It is clear that the beam-rod analogy exhibits the same type of loss mechanisms. Thus, it is evident that its correspondence with ferromagnetic behavior is tight. It also seems altogether reasonable to postulate these mechanisms as being responsible for hysteretic effects in general. Indeed, it appears that such effects have been observed in at least one other context--the elastic behavior of solids¹⁵.

2.2. The Resh-Preisach Plane

A one-to-one correspondence can be set up between the model and a parameter plane with an associated distribution function. There are some points of similarity with the plane of Preisach's model, but the interpretation of the distribution function is different. This will become clear subsequently.

Consider the plane sketched in Figure 2.2.1.

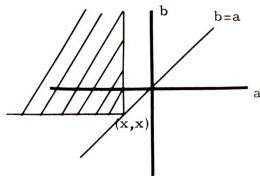


Figure 2.2.1

Each beam in the model can be represented as a point in the plane plus a number representing its coefficient of elasticity. If a beam in the model has equilibrium position a_i , drop off point b_i , and

elasticity coefficient K_i , it will be represented by a point (a_i, b_i) in the Resh-Preisach (or RP) plane. The point in the plane and the constant K_i suffice to characterize the beam. The rod position x can be represented as a point on the a axis. If the rod has increased its position monotonically from $-\infty$ to x , the resultant force on it will be the sum of the forces due to those beams which have been engaged but not dropped. Mathematically, such beams can be described as those with $a_i < x$ and $b_i > x$. In the plane, such beams occupy the shaded region of Figure 2.2.1. A moments reflection will reveal that the half-plane above the $b = a$ line represents right-active beams, and the lower half-plane left-active ones.

The preceding state of affairs is evidenced when the rod moves monotonically from $-\infty$ to x . Suppose now that it increases monotonically from $-\infty$ to x_0 and then decreases from x_0 to $x < x_0$. The rod will then start to "back off" from those right-active beams still engaged at x_0 , and it will begin to acquire new left-active ones. This situation is sketched in Figure 2.2.2, with the shaded regions again representing active beams; that is, those which are engaged and delivering a component of force to the rod.

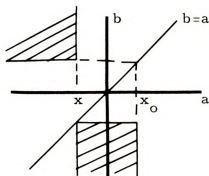


Figure 2.2.2



Following this line of thought, one can break up any continuous input function into monotone segments, thus determining the region of active beams for a given input function at any instant of time.

One of the most important effects which any model should exhibit is that of cyclic demagnetization. Resh demonstrated such an effect for the beam-rod model by assuming an input possessing a sequence of adjacent intervals of monotonicity (of alternating senses), such as a sinusoid, whose peaks smoothly decreased in amplitude from infinity to zero. The resulting region of active beams is shown in Figure 2.2.3. In like fashion, one can demonstrate cyclic magnetization effects, a virgin magnetization curve, and the cyclically demagnetized remagnetization curve.

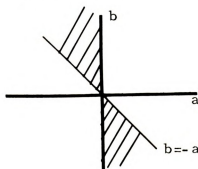


Figure 2.2.3

2.3. Mathematical Development

It is possible, then, to determine the region of active beams for any given input function and any instant of time. The primary item of interest, however, is the force versus displacement function. The past discussion has centered about intrinsically geometric factors: the beam equilibrium positions, their drop-off points, and the position of the rod. At this juncture, the question of magnitudes must be answered. How does the distribution of coefficients of elasticity from one beam to another influence the force versus

displacement relationship? Before exploring the possible answers to this question, a detour will be made for the purpose of developing a continuous version of the model.

In order to facilitate later investigation, it is essential that the model be generalized. Suppose the number of beams is allowed to approach infinity and each coefficient of elasticity allowed to tend to zero in such a way that the effective coefficient of elasticity per unit area of planar surface remains constant. In this manner, one is led to consider a continuous model. A function ϕ can then be defined on the plane such that $\phi(a,b) da db$ is the effective elasticity coefficient of a beam at (a,b) equivalent to the mass of ϕ in a rectangle with centroid at (a,b) and sides of length da and db . Consideration of the force due to one such element and summing over all such infinitesimal elements yields the force:

$$f(x) = \iint_Q (x - a) \phi(a,b) da db$$

where Q is the active region as previously defined, but extended to the continuous case.

The continuous model is appealing; for on a macroscopic level, an actual ferromagnet does exhibit smooth behavior--the discontinuous structure is of a "fine grain" nature. In addition, the continuous model provides an effective tool for both conceptual and computational purposes. Although the beams in the model have lost their structural identity in the transition to the continuous model, the terminology will be retained. The background idea is that the model has a basically discrete character, but that the number of beams is so large that it is more convenient to think in terms of a continuum.

Returning now to the discrete model, it is evident that the total force on the rod is the sum of the forces due to the active beams:

$$f(x) = \sum_{\substack{\text{Active} \\ \text{Region}}} (x - a_i) \cdot K_i$$

where the parameters are the same as before. It is possible to re-write this as

$$f(x) = \sum S_i K_i (x - a_i)$$

where the sum is taken over the entire planar aggregate, and S_i has the appearance of a state variable associated with the i^{th} beam:

$$S_i(x) = \begin{cases} 0; & \text{beam } i \text{ unengaged} \\ 1; & \text{beam } i \text{ engaged} \end{cases}$$

The corresponding state-like variable of the entire model is then the Cartesian product of the individual ones, and it can be written as a vector

$$\bar{S} = [S_1, S_2, \dots, S_N]^T.$$

The above expression is an input-output state relation and takes the form

$$f(x) = \bar{S}^T K(x \cdot \bar{1} - \bar{a})$$

where $\bar{a} = [a_1, a_2, \dots, a_N]^T$, $\bar{1} = [1, 1, \dots, 1]^T$, and

$$K = \begin{bmatrix} K_1 & 0 & \dots & 0 \\ 0 & K_1 & \dots & 0 \\ \vdots & \vdots & \ddots & \vdots \\ 0 & 0 & \dots & K_N \end{bmatrix}.$$

With the input-output state relation disposed of, it becomes necessary to determine a state transition function or algorithm. This is necessary for the unique determination of the force in terms of the displacement. Although it is possible to go through an active beam pattern analysis for each monotone segment in an input function, the nature of the state vector indicates the utility of a modular approach. Each beam can be analyzed for state transitions and then incorporated back into the aggregate to determine the overall state transition.

The above plan of attack requires a state model for an individual beam. Since there are two types of beams, there are two varieties of state model. Some consideration of the beam-rod analogy reveals the efficacy of the following pair:

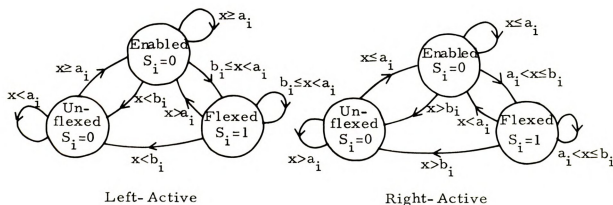


Figure 2.3.1

As an example, consider a right-active beam. If the beam is un-flexed, S_i is zero. If the rod position is greater than the equilibrium position of the beam, the state will remain the same. This will obtain until the rod position becomes less than the equilibrium position of the beam, in which case the state goes to "enabled" and S_i remains

zero. Then any motion of the rod back above the equilibrium position will cause the beam to enter the "flexed" state, with $S_i = 1$. Similar verification can be made for the other transitions shown.

In actuality, it is evident that S_i is not a state variable. It is a function defined on the state space of beam i . The state of a beam can be written as a variable which assumes the values Flexed, Unflexed, or Enabled. If S_i were invertible, it would also qualify as a state variable. Unfortunately, this is not the case, but the vector S serves essentially the same function as a state vector in the input-output state relation. The state vector of the model is a vector consisting of the entries Unflexed, Enabled, or Flexed in each position. At any rate, a complete state model is available for the finite beam discrete analogy.

2.4. The Process Model

It is possible to derive a model for the ferromagnetic process which is a direct consequence of physical theory. Its very generality does not allow its use as a quantitative solution, but its conceptual power will be evident. It is introduced here to coalesce all the models which have been discussed (including the beam-rod analogy) and to provide a framework for their comparison.

Consider the magnetization process for a uniform ferromagnetic toroid which is isotropic and homogeneous. If a current carrying conductor of small diameter is wound around the torus, the applied field intensity can be shown to be axial with respect to its cross section. In consequence of this, as well as the absence of physical boundaries, the magnetization is uniform.

The current carrying conductor produces a magnetic field intensity $H = B_a/\mu_o$, where B_a is the induction which would result if the torus were not present. The factor B_a (or H) can be considered as the motivating force for the ferromagnetic process. This disturbing influence causes the magnetic dipoles to begin to align themselves as outlined previously. This creates a resultant induction field which adds to B_a . This perturbed field creates further alignment, and so on. The resulting process-derived model is outlined in Figure 2.4.1.

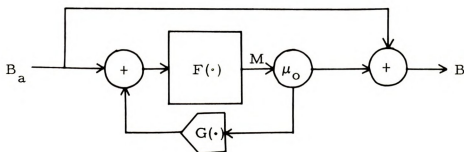


Figure 2.4.1

As indicated, the operator F is a functional relationship between the resultant induction field and the magnetization M . Note that this model is only valid if the magnetization can be characterized by a single number. In particular, if M is a spatial variant, the induction field at a particular point depends upon the entire distribution of magnetization.

Consider now the relation between this general model and those previously outlined. Suppose first that the operator F is given by

$$F(x(t)) = - \int_{-\infty}^t \phi(t, \tau) x(\tau) d\tau$$



and $G \equiv 1$.

Then,

$$M(t) = - \int_{-\infty}^t \phi(t, \tau) \left[B_a(\tau) + \mu_o M(\tau) \right] d\tau$$

But $B(t) = B_a(t) + \mu_o M(t)$, so

$$\mu_o^{-1} \left[B(t) - B_a(t) \right] = - \int_{-\infty}^t \phi(t, \tau) B(\tau) d\tau$$

or finally,

$$H(t) = \mu_o^{-1} B(t) + \int_{-\infty}^t \phi(t, \tau) B(\tau) d\tau$$

which is precisely Volterra's equation. Thus, Volterra's model is the special case which results when the operators F and G assume the special form indicated above.

Now consider Chua's model. The proposed differential equation

$$\frac{dy}{dt} = g \left[x(t) - f(y(t)) \right]$$

can be interpreted as a representation of the following system:

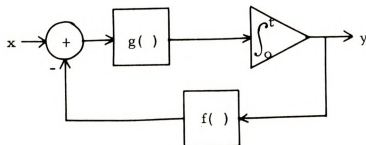


Figure 2.4.2

This model can also be brought into agreement with the process model. One feature, though, is clear--since there is no additive term proportional to the input, the output variable of this model



must be considered as corresponding merely to the magnetization M. The correspondence with the process model is clear. In this case,

$$F(x(t)) = \int_{-\infty}^t g(x(a)) da$$

$$G(x(t)) = f(x)$$

What of the current model under investigation? Inasmuch as it is a physical analogy, rather than a mathematical abstraction, the correspondence is not readily brought to light. In spite of this, there are several salient points to be noted. The model is an attempt to represent the driving forces--the causative agents--of the ferromagnetic process. This includes the basic operator and the feedback configuration, not merely the forward path alone. The additive term proportional to the input can be automatically taken care of by virtue of the elastic character of the constituent beams. Prior models have generally, in the context of the process model, consisted of specialized assumptions about the nature of the operators involved. The beam-rod model undertakes the general synthesis of those operators under the one assumption that they can be represented by an aggregate of elemental beams. The previous discussion of the correspondence between those processes at work in the model and those inherent in ferromagnetic action bodes well for such a modeling attempt.

2.5. Preliminary Results and Characteristics

As described in Resh's 1969 paper, a heuristically synthesized model was available at the inception of this work, although the order of the model was low. It produced a reasonable hand-calculated

saturation loop and crude cyclic demagnetization effects. In an effort to extract as much information as this model would yield, a discrete state simulation model was programmed for the finite beam analog. This algorithm, utilizing the previously described state model, is presented in Figure 2.5.1. An input-output characterization for each of several different inputs was derived in the form of a computer generated plot. Some of these characteristics are demonstrated in the figures immediately following 2.5.1.

Although there are several different possible correspondences between model and ferromagnet in terms of terminal variables, it is natural on several accounts to take the force f as analogous to H , applied field intensity, and the rod position x as analogous to B , the magnetic induction. The voltage versus current characteristic of an iron core inductor, then, would be obtained by allowing H to be proportional to the current I and differentiating the B variable to obtain the voltage.

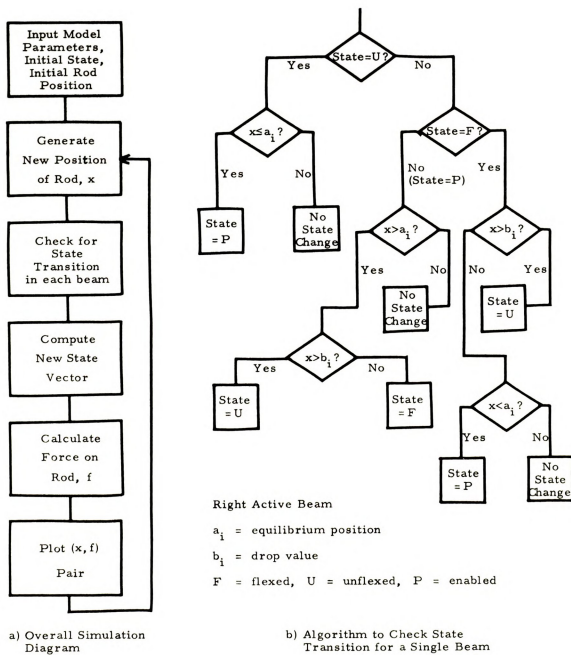


Figure 2.5.1

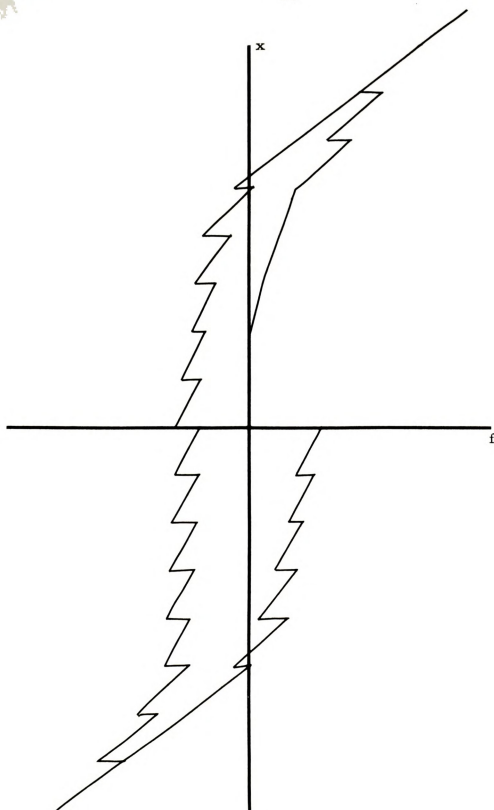


Figure 2.5.2

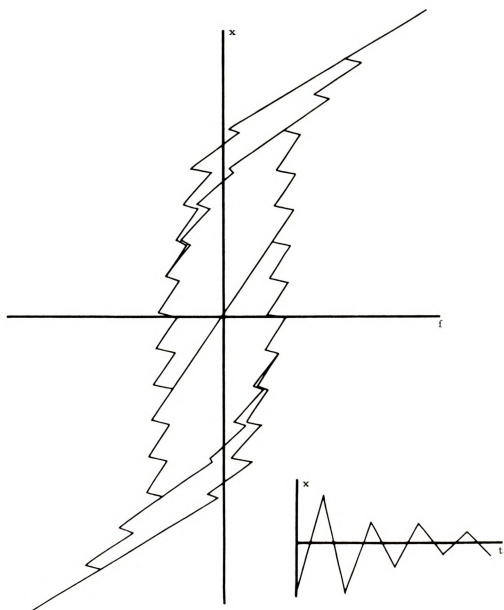


Figure 2.5.3

CHAPTER III

SYNTHESIS OF THE MODEL

3. 1. The Definition of the Problem

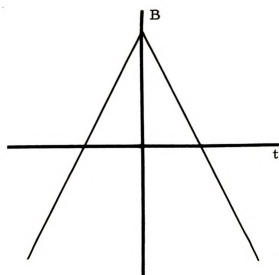
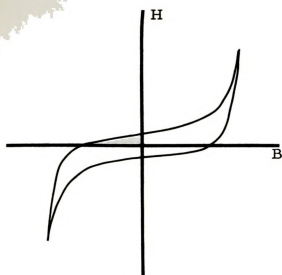
In order that an iron core inductor or other hysteretic ferromagnetic device can be incorporated into a larger network for simulation purposes, it is essential that the model parameters be known quantitatively. In particular, this means knowledge of the beam elasticities, equilibrium positions, and drop-off points for the discrete model or the distribution function ϕ for the continuous case. In either event, an experimental technique must be available for obtaining pertinent measurements on a particular device. It would be most desirable for measurements on a single specimen of a given type of material, say Arnold Deltamax, Permalloy, or the like, to yield a model valid for all members of that category. A final answer to this must await experimental verification, but this chapter outlines a measurement technique which effectively yields the model parameters. The main objective of the discussion at hand, then, is the delineation of a synthesis procedure which accepts these measurements and produces the desired parameters. The work embodied in this thesis will be concerned with synthesizing these parameters on the basis of static or dc measurements. Incorporation of frequency effects should be looked upon as an extension of the current effort.

The investigation of a problem of this nature necessarily entails the question: What are the general characteristics of the device

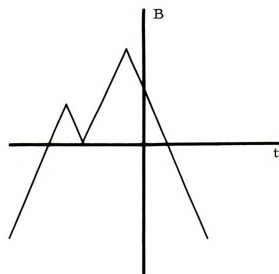
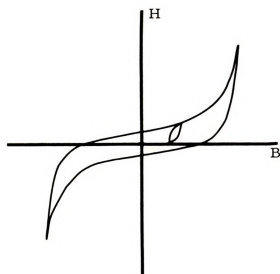
whose model is to be synthesized? For the case at hand, there is no simple answer. Physicists have purveyed a dark pessimism with regard to such a description. In fact, one writer¹⁶ goes so far as to aver, "... even the simplest B versus H curves conceal a lot of complicated events. It is not surprising, then, that efforts to use empirical formulas to describe such curves... are doomed to failure." The allusion is to such tired workhorses of engineering-oriented magnetic theory as the Law of Steinmetz.

In spite of the above pessimism, an abundance of insight is afforded by the subjection of the device to a wide range of input time functions. Plotting the output versus input gives rise to a set of planar relations. Upon inspection of a large sample of such relations, a number of regularities emerge. For example, all inputs which increase monotonically from a large negative value, to a large positive value, thence to another large negative value result in the same relation--that of Figure 3.1.1(a). The precise meaning of "large" will be clear from subsequent elaboration. Figures 3.1.1(b) and 3.1.1(c) indicate other such categorical features.

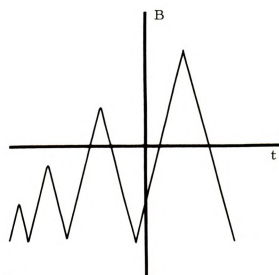
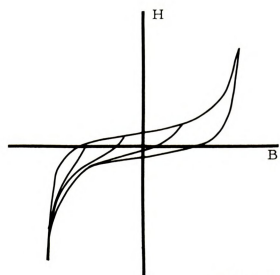
The process of constructing a model on an ad hoc basis when a finite number of input-output relations are given is often termed behavioral modeling. Theoretically, if an infinity of such relations are determined for inputs ranging over the class of all such possible, the model will be ideal. This means that the output can be determined from such a model for any input which the environment can supply. Since such a characterization is obviously impractical, one must content himself with more miserly results. One of the first features to note, in a search for a more practical approach, is the concept of



Saturation Loop



Minor Loop



Semimajor Loops

Figure 3.1.1

equivalence mentioned above. This concept is inextricably intertwined with the idea of state, but for present purposes, the major import lies in the reduction of the number of relations which must be investigated. If an increasing set of input-output relations is determined, it should be a requirement that the resulting models converge, in some fashion, to the ideal. Another salient point is the following. If a given behavioral model possesses close ties with known physical processes at work within the object, the validity of the model can only be enhanced. This desirable quality is one feature inherent in the model under investigation here.

These few remarks are intended as a prelude and delineator of the work to follow. At various stages in the development, some commentary will be made to correlate current aspects with these remarks.

3.2. Experimental Measurements

As pointed out in the preceding section, laboratory measurements must be performed on a given device in order to obtain input data for a synthesis procedure. Such measurements need be exact only to a degree relative to the precision of the synthesis routine. No attempt is made in this thesis to provide numerically precise tolerances, so the main interest will focus on the development of suitable techniques of measurement.

The terminal variables of interest are current and voltage in the case of an iron core inductor. The point was made previously, though, that the choice of current and flux linkage is more appropriate to the model. The terminal voltage, of course, is obtainable from the flux linkage by differentiation.

The preponderance of iron core inductors are of the closed flux variety. This means that the continuous flux paths lie entirely (for all practical purposes) within the ferromagnetic core of the inductor. A smaller number of practical inductors are of an open flux nature. Flux measurements for the latter are not difficult at either dc or higher frequencies. The discussion will center generally about the closed-flux type of inductor and specifically upon the toroidal form. The uniformly wound toroid with its lack of normal surfaces, has the nice aspect of possessing uniform magnetization. Ac measurements are not difficult for the torus, but dc tests are exceedingly difficult. The closed nature of the flux paths preclude utilization of any such device as a Hall-effect or magnetometer probe. The common method of ac testing involves driving one winding of the toroid with a periodic current, then integrating the voltage induced in a sense coil. This provides a voltage proportional to the flux change in the toroidal core. The test configuration is shown in Figure 3.2.1.

This type of setup works well for ac measurements; in fact, a common RC integrator can be used at the higher frequencies. Since the voltage induced in the search coil is proportional to the time derivative of the flux, a slowly varying, or "dc", input current will result in a miniscule output voltage. Another shortcoming is the decay time, or holding time, of the integrator. When the input to the integrator changes and then goes to zero for a long period of time, the integrated value decays toward zero. Several attempts have been made to obtain satisfactory integration at these low rates of change of the input. The most effective solution to date has been

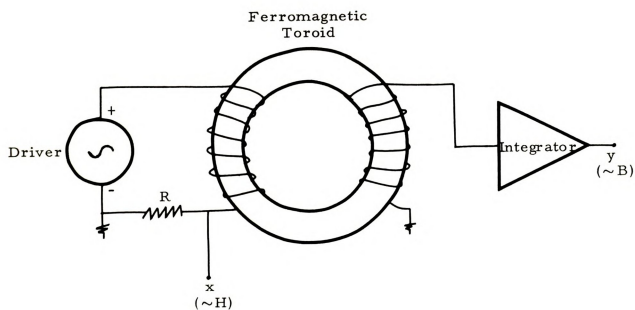


Figure 3.2.1

the use of ballistic galvanometers^{16, 17, 18} with feedback to obtain high integrator accuracy. These instruments are very delicate, so a more robust integration unit is desirable.

The techniques for obtaining practical integration are explored in the appendix. At this juncture, it is sufficient to state that dc tests are practical. In fact, using the experimental arrangement illustrated in Figure 3.2.2, it was found feasible to manually control the driving current into the toroid and concurrently plot the input-output characteristic by means of an x-y recorder. Several relations of interest are shown in Figures 3.2.3 through 3.2.6 for two radically different types of core material--one square loop and the other of softer material. One feature resulting from these experimental investigations is at variance with the work of previous inquirers. At dc, minor loops close immediately and do not approach such a loop only as a limit. It seems suspect that lack of immediate closure is an ac effect, perhaps caused by eddy currents.

3.3. The Search for the Support of the Distribution Function

With measurement techniques available, it is now possible to break the theoretical soil with confidence. As a cornerstone for the analytical framework, these experimental techniques provide some of the coarser characteristics which the beam-rod model must exhibit. The first logical step would seem to be the query, "What coarse characteristics of the model give rise to these coarse experimental features?" This is indeed a logical question, and a solid answer to it is available.

One of the most general characteristics of the model is the support of the distribution function ϕ . The support of ϕ is defined by

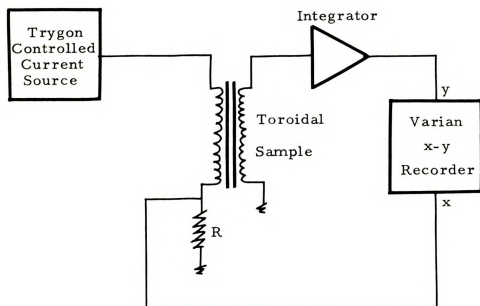


Figure 3.2.2

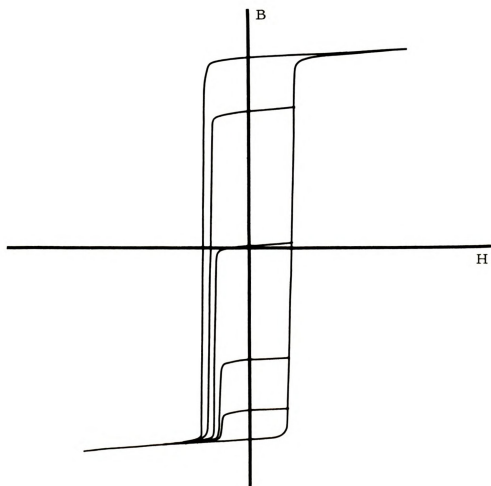


Figure 3.2.3

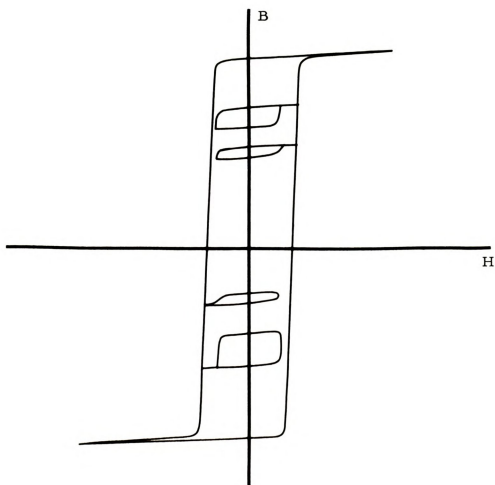


Figure 3. 2. 4



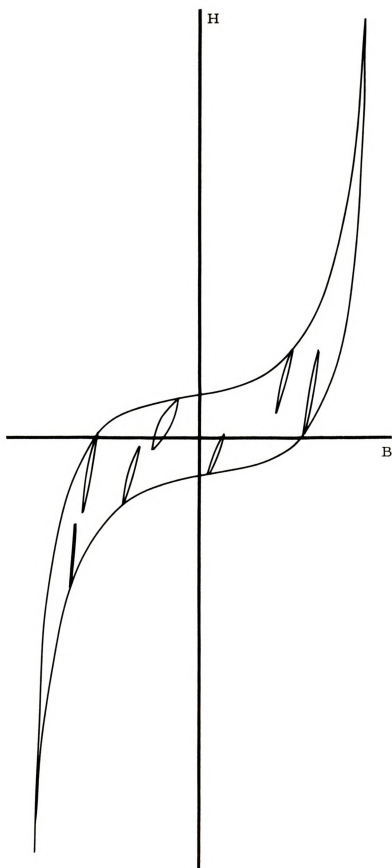


Figure 3.2.5

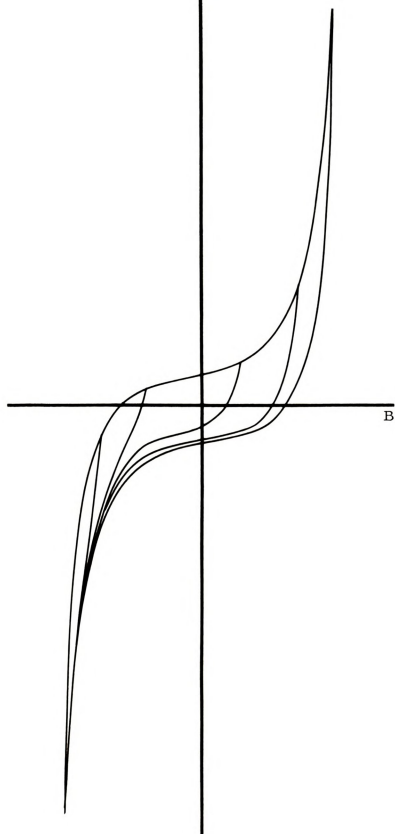


Figure 3. 2. 6

$$S(\phi) = \{ (a,b): \phi(a,b) \neq 0 \}$$

It is plausible that $S(\phi)$ could be the entire plane, but it seems intuitive that this is not the case. It would be convenient, in the light of later developments, if the support were a compact set. In any event, it is certainly reasonable to postulate a region for the support and subject it to experimental test. Such a procedure bears fruit in the current investigation and, as will be argued later, produces a logically palatable result.

It is perhaps wise at this point to inventory the available tools. There are two of major importance: the heuristically synthesized finite beam model provided by Resh and the previously outlined discrete state simulation algorithm. The extant model, though of low order, gave important clues. In the first place, there was a region of regularly spaced beams with identical coefficients. This was concluded to account for the behavior observed in the "body" of the characteristic, that is the state determined portion. It is helpful to study the planar description of the model which is provided in Figure 3.3.1. Another category of beam possessed very large drop values, and their coefficients varied in a rather precipitous manner from one beam to its neighbor. It was felt that these "boundary" beams accounted for the overall shape by virtue of their nonlinear behavior, and for the behavior in the saturation region by reason of their large drop values.

Resh's model provided nice results as far as the saturation loop and magnetization curve were concerned, but minor loop behavior was relatively crude. Cyclic demagnetization effects were in evidence, but they too were of a somewhat crude nature. These strong

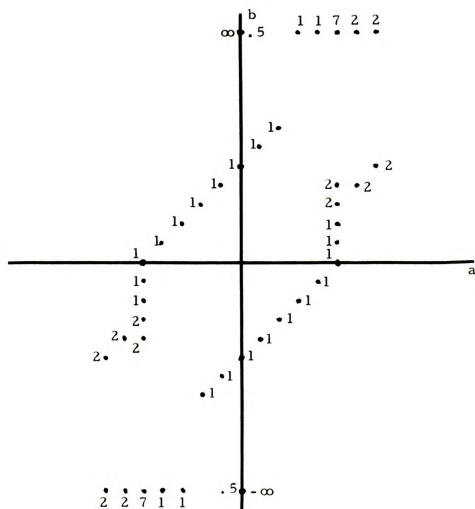


Figure 3.3.1

but coarse correspondences seemed evidence of the correct nature of the accompanying approximation to $S(\phi)$. The prominent features of this approximation are:

1. It consists of the union of three regions, one with finite drops and the other two with very large, perhaps infinite, drops.
2. There are no beams with equilibrium positions larger in magnitude than the saturation value of displacement.

With these features in mind, it was decided that the correct approach was to perturb the parameters of Resh's model and investigate, using the finite state algorithm, whether the results were a refinement or a degradation. The simulation results were obtained in the form of a computer generated plot of an input-output relation. A standard piecewise-linear driving function was selected such that sufficiently rich hysteretic behavior could be observed. The first perturbation was of a minor nature: the constituent beams were merely multiplied in number along the linear geometry of the original model, with the total coefficient per unit length remaining the same. The resulting perturbation is shown in Figure 3.3.2, and the simulation result in 3.3.3. The results were essentially the same as for the original. There was a marked increase in smoothness, although the cyclic demagnetization effects and minor loops were unimproved.

The next perturbation was more pronounced. The original model outlines were retained, but this basal skeleton was filled with equally spaced beams of constant coefficient. The boundary beams were retained intact, for the overall shape of the saturation loop was

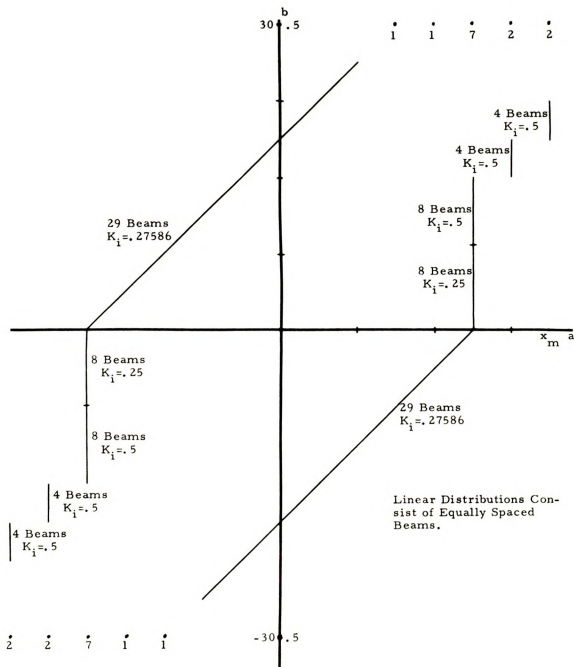


Figure 3.3.2

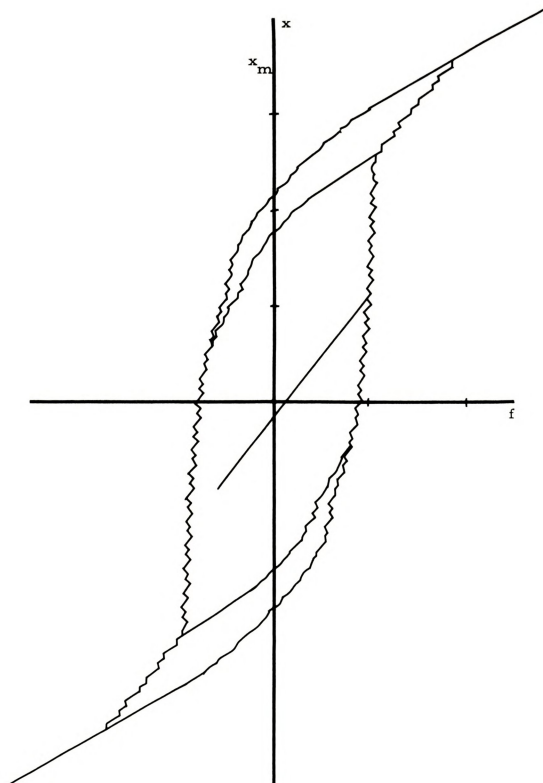
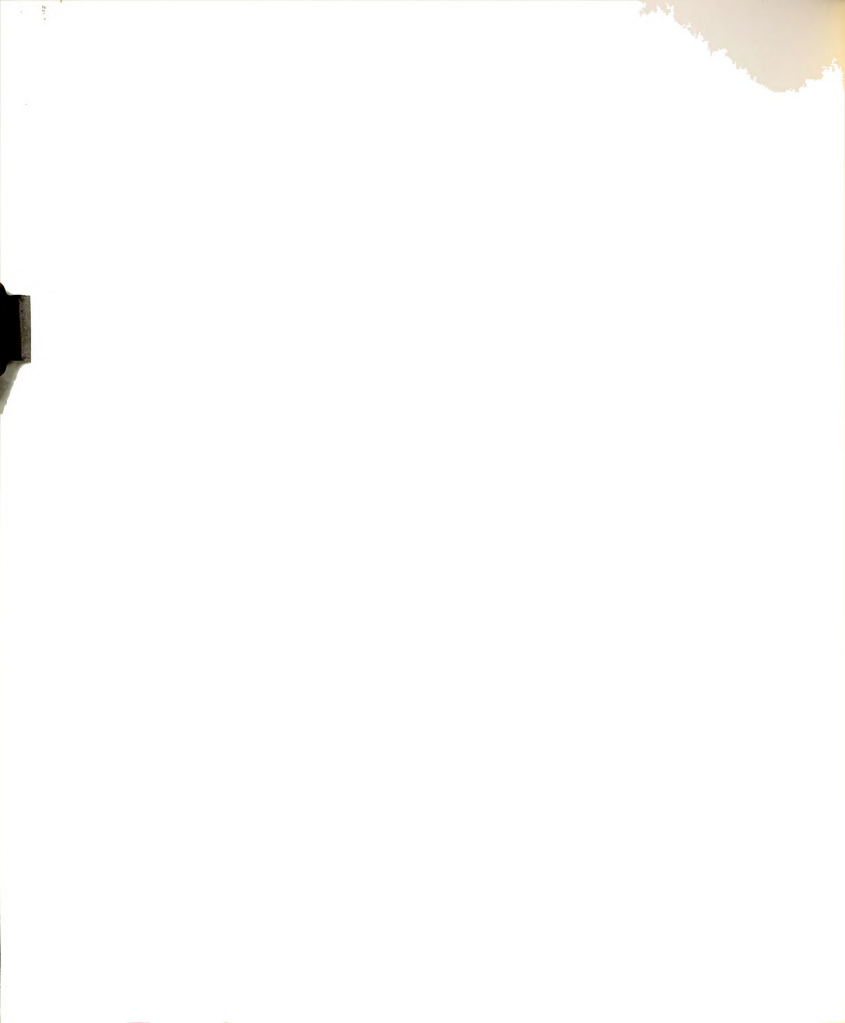


Figure 3.3.3



correct. These results are presented in Figures 3.3.4 and 3.3.5. There was a dramatic increase in overall smoothness, as well as in cyclic demagnetization effects. The latter, however, seemed to possess some undesirable characteristics which were remarkably tenacious. The semimajor loops refused to produce sides which were distinct from those of the saturation loop. Upon consideration of the Resh-Preisach plane, it was felt that beams must be present at points well away from the $b=a$ line in a perpendicular direction in order to provide more reasonable interior loops.

In keeping with this attitude, the next perturbation was even more of a departure. Body beams were arranged in the configuration of a square centered at the origin with sides of length $2x_m$ (x_m being the saturation value of displacement). The perturbed geometry and the simulation results were those of Figures 3.3.6 and 3.3.7. Although the overall shape was completely distorted, the minor loop behavior appeared to be very much like that sought.

After performing a number of more detailed perturbations and simulations, one fact seemed clear. A trade-off of some nature was needed between the models of Figures 3.3.4 and 3.3.6. But how is a trade-off between two geometric patterns to be accomplished? After some thought, the answer presented itself--simply increase the vertical dimensions of Figure 3.3.4. Then a square of beams (Figure 3.3.6) would be imbedded in a trapezoid of beams (Figure 3.3.4). The result is indicated in Figure 3.3.8. Figure 3.3.9 contains the resulting simulation relation. Cyclic demagnetization loops and overall shape appear correct, but there are undesirable discontinuities in the saturation region.

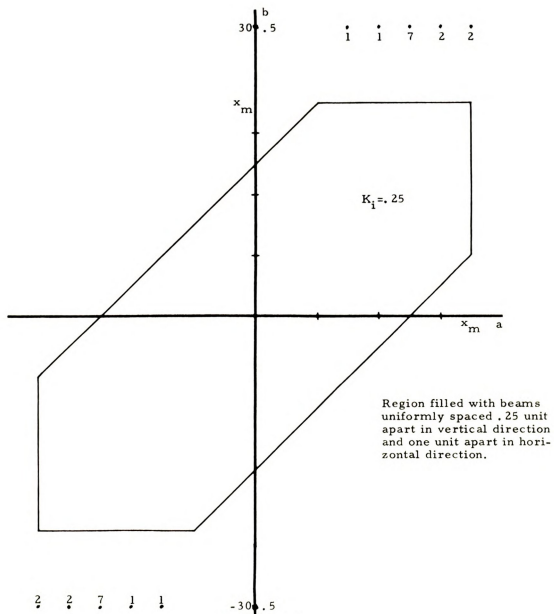


Figure 3. 3, 4

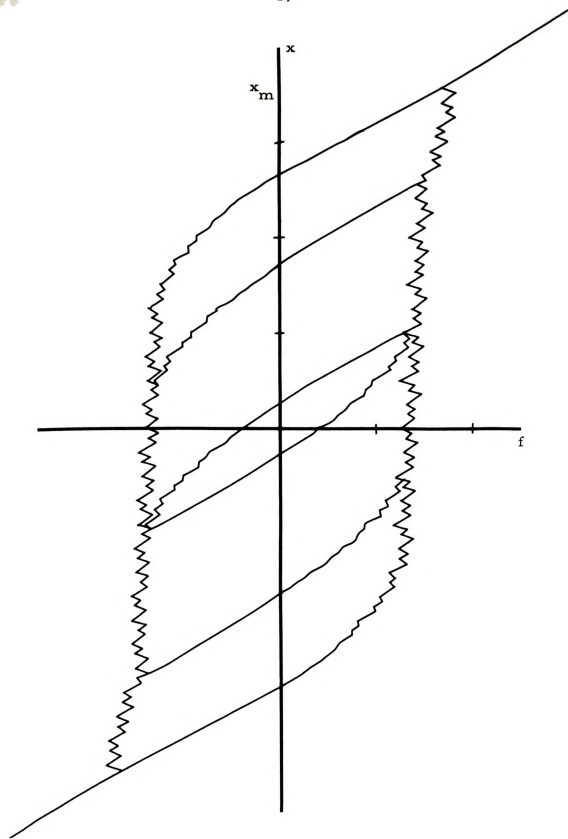


Figure 3.3.5

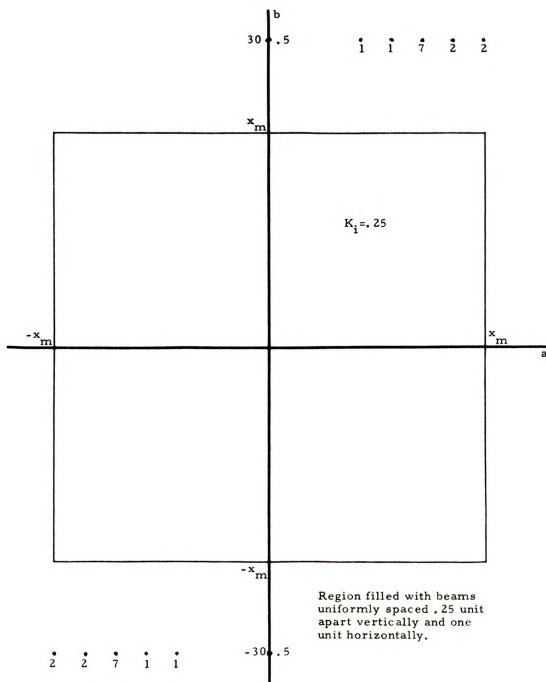


Figure 3.3, 6

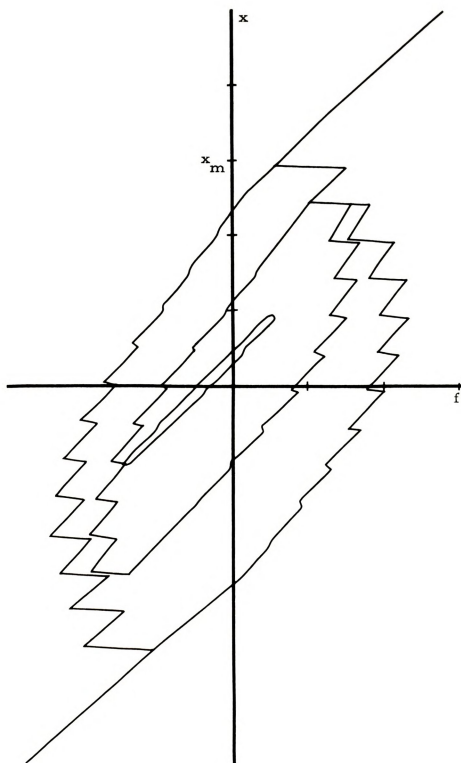
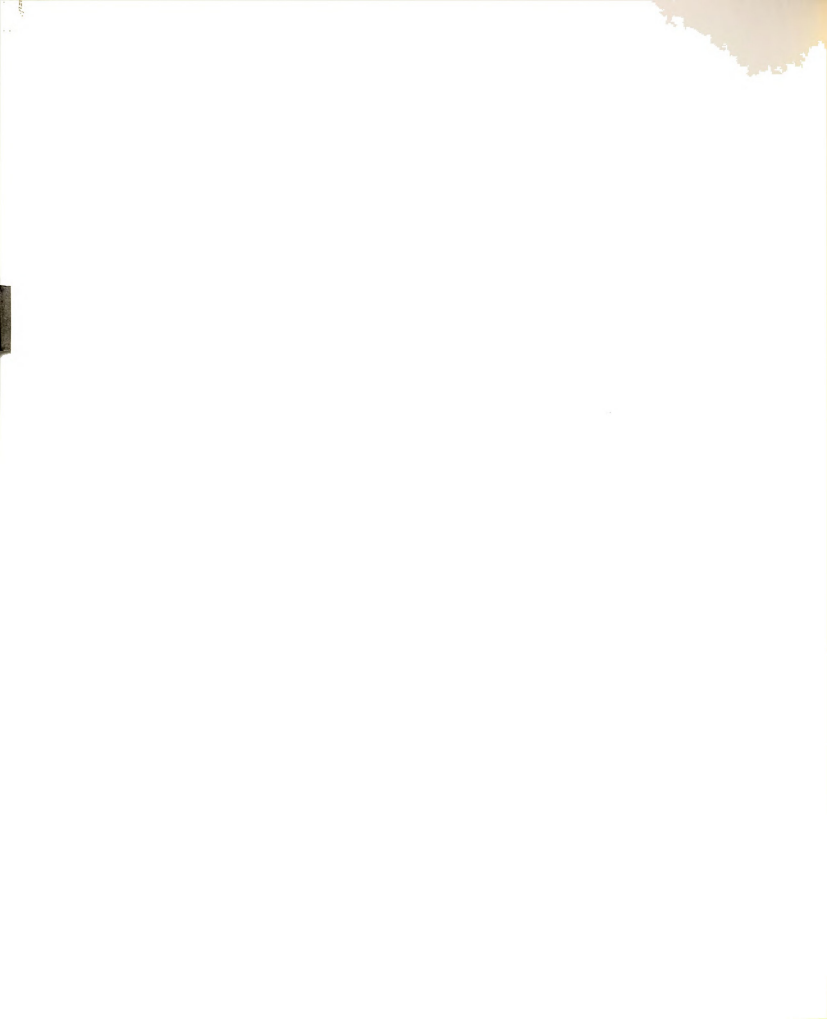


Figure 3.3.7



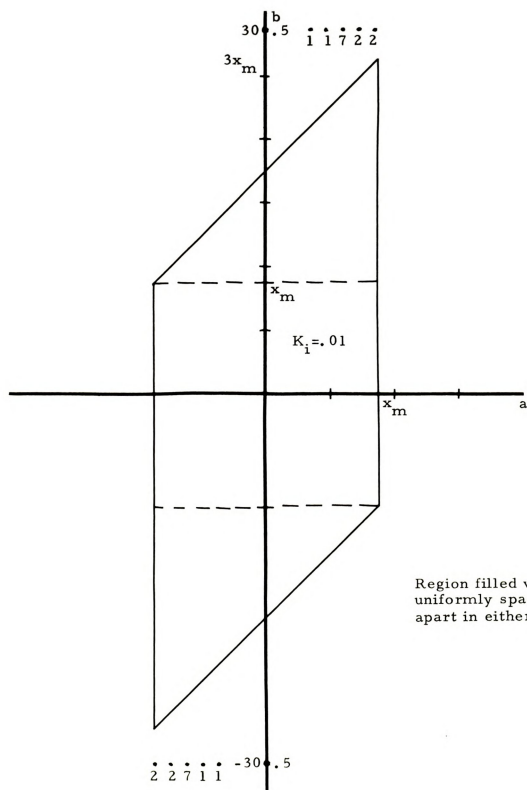


Figure 3.3.8

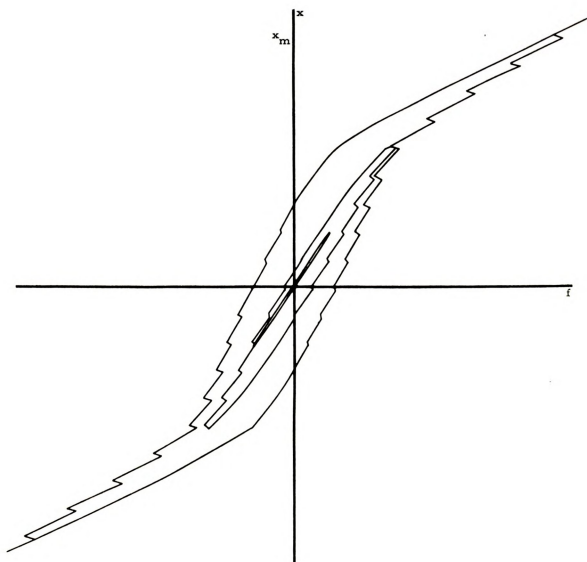
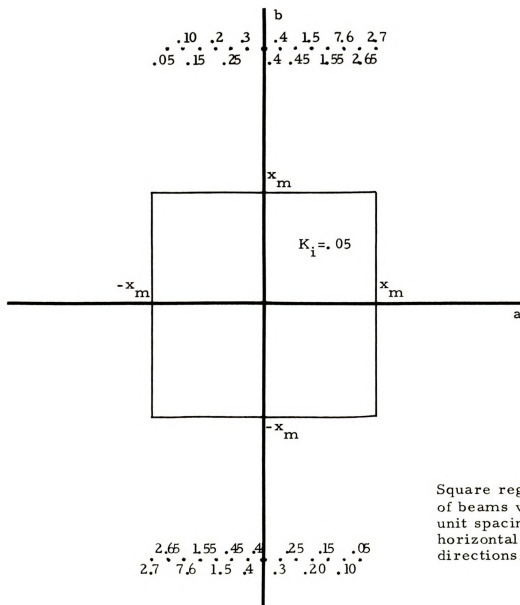


Figure 3.3.9

The final solution is now at hand. By splitting the preceding trapezoidal region into three parts, as indicated by the dotted lines in Figure 3.3.8, the cyclic characteristics of the square are retained, and the overall shape is maintained, while the discontinuities in the saturation region have been deleted. The beams previously contained in the top and bottom triangular components are moved into positions with very large drop values. The final configuration is shown in Figure 3.3.10, and its characteristics are depicted in Figure 3.3.11.

One final facet should be pointed out at this stage of development. A given finite beam model can be improved dramatically in fineness by simply spreading the beams in a vertical direction. This distributes the drop points, and thus the discontinuities, over an interval rather than concentrating them at a single point. Figure 3.3.12 is the simulation result of the same model as that of Figure 3.3.10 with a ten for one vertical spread in drop values. Note the decrease in the amplitude of the discontinuities.

Now that the extent of the support of ϕ has been delimited for the discrete model, it can also be enunciated for the continuous case. Figure 3.3.13 indicates the generic character of the most general possible structure of $S(\phi)$. The major features are as follows: There is a square region consisting of body beams. This region contains the memory elements of the model. There are two regions with infinite values of drop. Both have equilibrium position values distributed between $-x_m$ and $+x_m$, with x_m being the saturation value of rod displacement.



Square region consists of beams with uniform unit spacing in both horizontal and vertical directions.

Figure 3.3.10

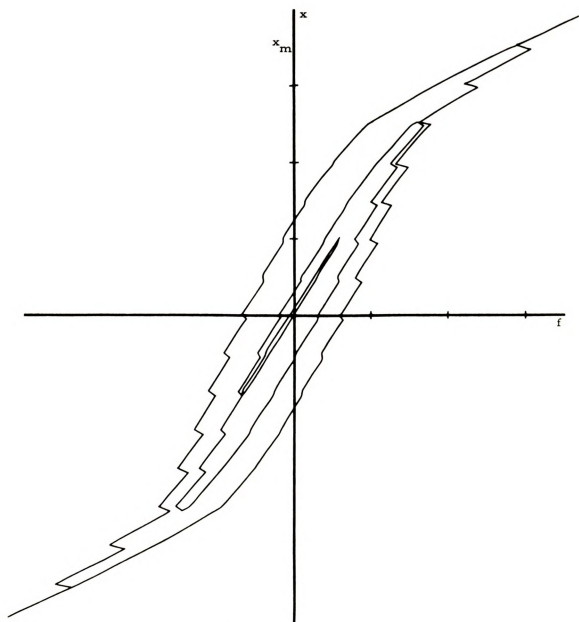


Figure 3. 3. 11

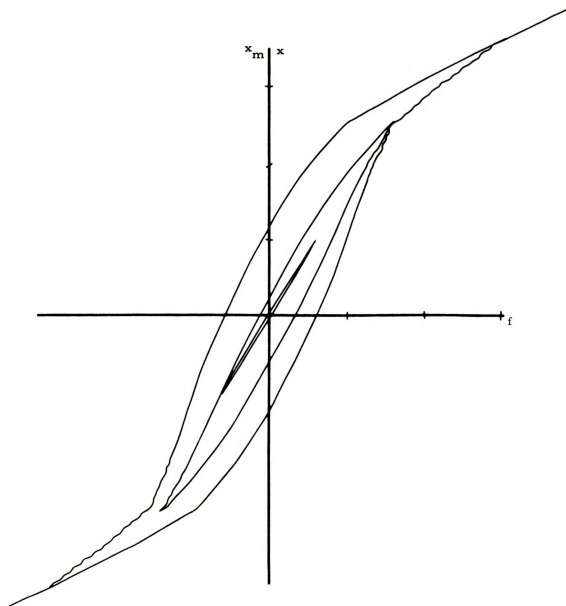
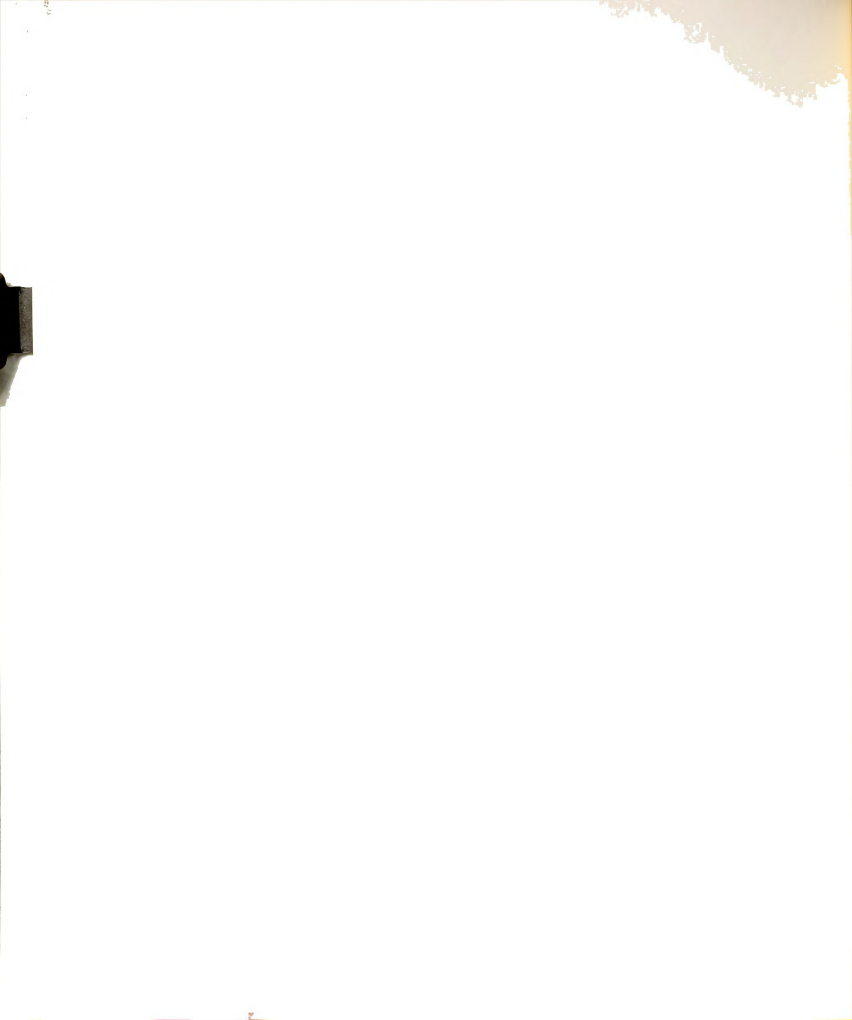


Figure 3. 3. 12



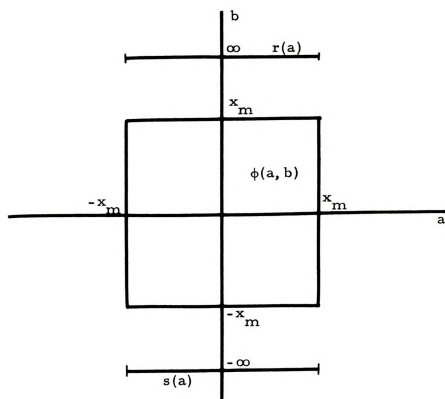
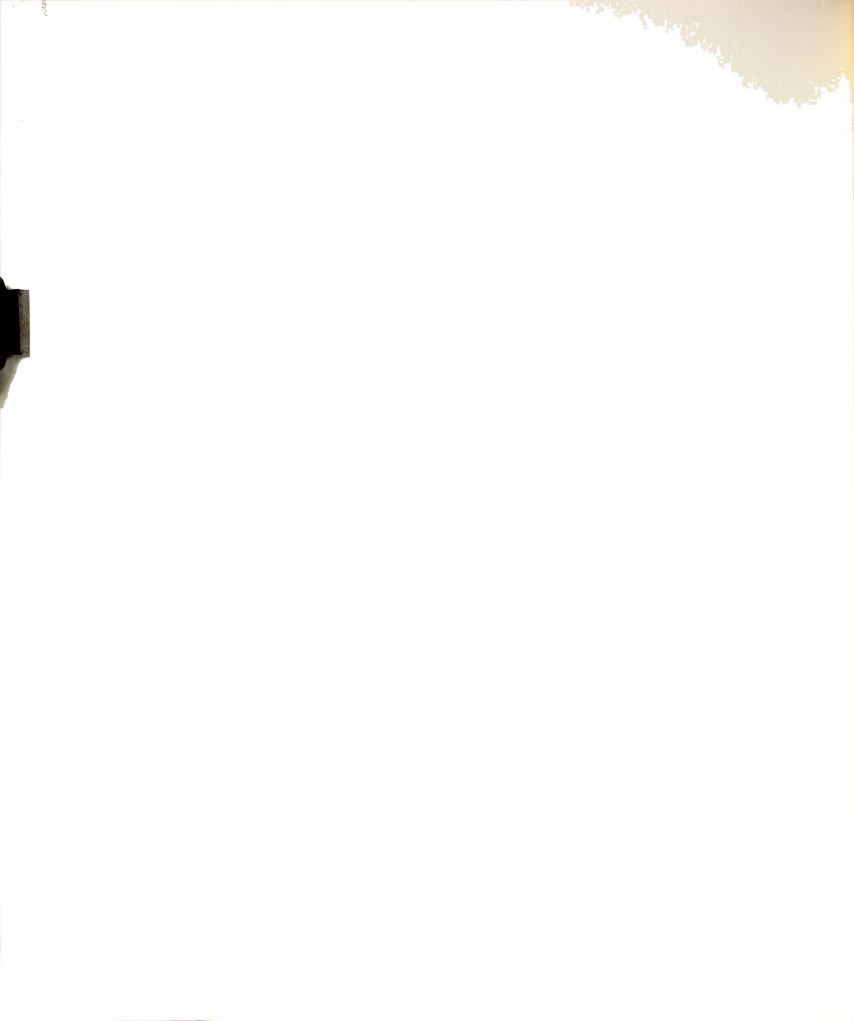


Figure 3.3.13



In accord with the previous allusion, this region for $S(\phi)$ is logically defensible. In fact, it could possibly have been deduced by proceeding from observed characteristics alone. Although the continuous model provides an accurate picture on a macroscopic level, the fine grain structure reveals basically discontinuous processes at work. These processes do not appear in the saturation region. Hence, in the model, no beams can be dropped for $|x| > x_m$. In addition, the input-output relation is linear in the saturation region. This implies that no additional beams are acquired for $|x| > x_m$. A farther feature is the fact that the relation does not consist of the horizontal axis (that is, the mmf, or force f , is nonzero) for $|x| > x_m$. This implies that beams with infinite drops do exist in the model. These facts coupled with a few thought experiments imply the region of Figure 3.3.13 for $S(\phi)$.

3.4. Synthesis Considerations

With the knowledge of the most general region possible for the support of ϕ , it becomes feasible to consider the more concrete problem of synthesizing the model parameters. As was indicated in Figure 3.3.13, it is convenient to think of ϕ as representing the beam mass distribution in the square, and of two other functions r and s as representing the two linear distributions at $\pm\infty$. When considering the discrete model then, it is convenient to simply imagine these functions as being evaluated at a finite set of points. If these values are multiplied by an area weighting factor, there arises a discrete approximation to the continuous model. This is simply the inverse of the process used to make the transition from the discrete to the continuous model. In fact, if the continuous model

can be synthesized, it is possible to immediately make such an approximation--thereby allowing the Barkhausen effect to reappear.

For the purpose of mitigating the synthesis problem as much as possible, it becomes desirable to farther simplify the model by introducing reasonable assumptions such as, for example, symmetries of the various distribution functions. An added simplification is possible for the boundary distribution functions. To investigate this, it is necessary to consider the expression for the force contributed by the boundary. This is readily seen to be

$$g(x) = \int_{-x_m}^x (x - a) r(a) da + \int_x^{x_m} (x - a) s(a) da$$

The corresponding expression for the discrete model is:

$$g(x) = \sum_{a_i \leq x} (x - a_i) r_i + \sum_{a_i > x} (x - a_i) s_i$$

where the a_i are the equilibrium positions for the discrete model and r_i and s_i are the elasticity coefficients of the top and bottom boundary beams.

It is interesting to consider the derivation of these boundary distributions if $g(x)$ is a prescribed function. Note that, on the contrary, $g(x)$ will not in general be known. The assumption is merely made for the purpose of deriving properties of the boundary distribution functions. Under this proviso, then, differentiating the first of the above expressions twice results in

$$g''(x) = f(x) + s(x)$$

The most striking feature here is one of redundancy: a single function would suffice. If either r or s were identically zero, the resulting force component would be of constant sign (assuming the other

function is always ≥ 0)-this conflicts with intuition and the underlying physical mechanisms. In fact, it would imply a very strong asymmetry in the saturation loop. Hence, it appears that r and s should possess an alternation property--that is both are never zero simultaneously. A more explicit form will be presented later.

Turning to the other simplification mentioned above, it is pertinent to inquire as to possible symmetry of the function ϕ . In measurements on actual devices, it is observed that should any sequence of inputs be negated in sign, the corresponding output function experiences a similar sign inversion. Since the boundary distribution is memoryless, a little thought will convince one that this sign characteristic should also hold for the force due to the function ϕ . One symmetry condition which furnishes this behavior is given by

$$\phi(-a, -b) = \phi(a, b)$$

It is possible to use this symmetry condition to explicate the nature of the boundary distribution. If the saturation loop is swept out, the resulting forces can be written:

$$f^+(x) = g(x) + \delta^+(x)$$

$$f^-(x) = g(x) + \delta^-(x)$$

where $f^+(x)$ and $f^-(x)$ are the saturation loop forces with x increasing and decreasing, respectively; $g(x)$ is the force due to the boundary distribution; and $\delta^+(x)$ and $\delta^-(x)$ are the body contributions, also for x increasing and decreasing, respectively. Now the symmetry condition $\phi(-a, -b) = \phi(a, b)$ implies that $\delta^+(x) = -\delta^-(-x)$. This can be seen by inspection of Figure 3.4.1. Then, manipulation of the above pair of equations results in

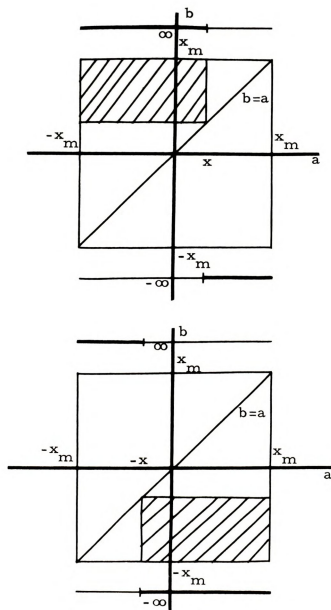


Figure 3.4.1

$$f^+(x) + f^-(-x) = g(x) + g(-x)$$

In light of the above discussion of the "oddness" of hysteretic behavior, $f^+(x) = -f^-(-x)$. Hence, $g(x) = -g(-x)$, and the function g is odd. This implies the boundary distribution indicated in Figure 3.4.2.

The basic characteristics of the model have been made concrete, and the stage is set for expounding the method of synthesis of ϕ and r . This question will occupy center stage in the next section.

3.5. Synthesis of the Distribution Functions

There are a number of techniques which suggest themselves as answers to the synthesis question. The prominent characteristic with which the successful candidate must be endowed is practicality. A number of different methods were considered along the path toward selection of the one presented in the sequel, but all others suffered badly when extracted from the theoretical world. In truth, several seemed quite attractive when considered from the viewpoint of mere theoretical plausibility alone. Their downfall came at the hands of the ever-present demand for reasonable core storage and computation time on the digital machine. The one presently to be described possesses reasonable characteristics in those areas; it also provides excellent synthesis capabilities.

One of the most reliable weapons in the numerical analyst's arsenal is the polynomial approximation. The usual usage is in providing an approximation to a scatter of data or to a more complex function. The main requirement which the data must meet is the possession of a compact support--if the fit is to approximate the entire data set. For instance, Weierstrass' Theorem in one

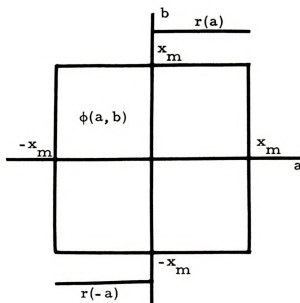
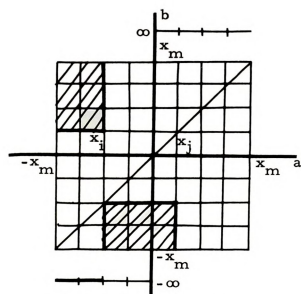


Figure 3.4.2

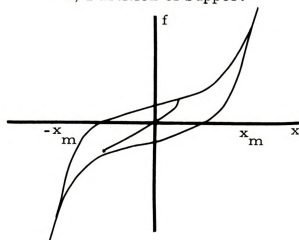
dimension is valid only for a closed interval of finite length. Of course, polynomial approximations are feasible in two dimensions, where the support must be a compact set. The importance of the previous effort in search of the support of ϕ is now apparent. The function ϕ is defined and nonzero only on the closed square (a compact set), and the function r is defined and nonzero only on a closed interval of finite length (another compact set). Thus, polynomial approximations would be practical if the functions ϕ and r were known. But, this is precisely the synthesis question itself! How then can the possibility of polynomial approximations be exploited?

Suppose the existence of such an approximation is assumed-- that ϕ and r are continuous. For a given degree of approximation, the problem devolves to one of determining a given number of coefficients. A number of measurements are needed which will allow these coefficients to be determined. The question is, "What kind and how many?" Of course, since a least squares solution is contemplated, the answer to the latter part is, "As many as feasible." To acquire a grasp on the former requires a little more effort.

With this objective in mind, consider the planar representation of Figure 3.5.1(a). The square is partitioned into N^2 equal subsquares, and the interval $(0, x_m)$ into $N/2$ equal subintervals (by construction N is even). The function ϕ is assumed to be represented by discrete beams centered in the small squares, and r by beams centered in the subintervals. If x is allowed to increase from $-\infty$ to x_j , then to decrease to x_i , those beams in the shaded regions will be engaged. This measurement process is illustrated in Figure 3.5.1(b). There are $(N(N-1))/2$ unknowns in the square and the same number of



a) Partition of Support



b) Semimajor Loop Measurements

Figure 3.5.1

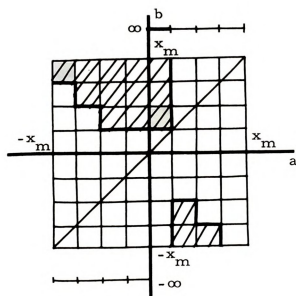
possible measurements. Note that those beams for which $b = a$ have no effect and can be ignored. The boundary beams, represented in continuous form by r , constitute an additional $N/2$ unknowns. Figures 3.5.2(a) and (b) represent a possible means for including an additional $N/2$ measurements by way of the cyclically demagnetized remagnetization curve.

The purpose of the preceding discussion is to motivate and heuristically justify the measurements to be performed for input to the continuous model synthesis procedure. There are $N^2/2$ measurements and $N^2/2$ unknowns. It seems that these $N^2/2$ measurements would suffice to determine the discrete model parameters, but their independence has not been verified. Fortunately, the synthesis procedure to be outlined does not require independence, although the supposition will be made that this type of measurements provides enough information for the continuous model. This, too, is non-critical, as will be brought to light later.

Although the measurements have been decided upon, the question of synthesis is still open. To fill this hiatus, the continuous synthesis procedure will now be explored. Utilizing the previously stated assumption of continuity of both ϕ and r , it is possible to hypothesize the existence of polynomials $P(a, b)$ and $Q(a)$ approximating ϕ and r uniformly to an arbitrary degree. Suppose

$$P(a, b) = \sum_{i=1}^{N+1} \sum_{j=1}^{N+1} a_{ij} a^{i-1} b^{j-1}$$

and
$$Q(a) = \sum_{i=1}^{N+1} b_i a^{i-1}$$



a) RP Plane

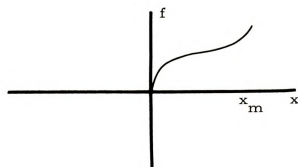
b) CDRC: Cyclically Demagnetized
Remagnetization Curve

Figure 3.5.2

where the range of indices has been selected for ease of programming on the digital machine. Then, the resulting approximation f' to the force versus displacement characteristic can be found for any sequence of input variations. For the set of measurements outlined above, there are four requisite force expressions: the ascending saturation loop, that due to decreasing input after a monotone increase from $-\infty$ to some value x_0 (semimajor loop); the cyclically demagnetized remagnetization curve (CDRC); and the force in the saturation region ($|x| \geq x_m$). The last form is obtained from any of the others by inclusion of only the expression for the force due to the boundary distribution. The different cases will be explored one by one, but first the symmetry condition on ϕ will be translated into a requirement on polynomial coefficients. The stipulation that $\phi(-a, -b) = \phi(a, b)$ implies that

$$\sum_{i=1}^{N+1} \sum_{j=1}^{N+1} a_{ij} \left[1 - (-1)^{i+j} \right] a^{i-1} b^{j-1} \equiv 0$$

Hence, $a_{ij} = 0$ if $i+j$ is odd. This will, of course, significantly enhance computation speed. The following expressions are derived from consideration of events in the Resh-Preisach plane.

The Ascending Saturation Loop:

$$\begin{aligned} f'(x) = & \int_{-x_m}^x da \int_x^{x_m} (x-a) P(a, b) db \\ & + \operatorname{sgn}(x) \int_0^x (x-a) Q(a \operatorname{sgn}(x)) da \end{aligned}$$

where the latter term is the boundary force, which can also be written in the less compact, but more intuitive form

$$g(x) = \begin{cases} \int_0^x (x-a) Q(a) da; & x \geq 0 \\ \int_x^0 (x-a) Q(-a) da; & x < 0 \end{cases}$$

Then,

$$\begin{aligned} f'(x) &= \sum_{i=1}^{N+1} \sum_{\substack{j=1 \\ i+j \text{ even}}}^{N+1} a_{ij} \int_{-x_m}^x da \int_x^{x_m} (x-a) a^{i-1} b^{j-1} db \\ &+ \sum_{i=1}^{N+1} b_i \cdot \operatorname{sgn}(x) \int_0^x (x-a) \left(a \operatorname{sgn}(x) \right)^{i-1} da \end{aligned}$$

or

$$f'(x) = \sum_{i=1}^{N+1} \sum_{\substack{j=1 \\ i+j \text{ even}}}^{N+1} a_{ij} H_{ij}(x) + \sum_{i=1}^{N+1} b_i B_i(x)$$

where

$$H_{ij}(x) = \int_{-x_m}^x da \int_x^{x_m} (x-a) a^{i-1} b^{j-1} db$$

and

$$B_i(x) = \operatorname{sgn}(x) \int_0^x (x-a) \left(a \operatorname{sgn}(x) \right)^{i-1} da$$

Semimajor Loop:

$$\begin{aligned} f'(x) &= \int_{-x_m}^x da \int_{x_0}^{x_m} (x-a) P(a, b) db + \int_x^{x_0} da \int_{-x_m}^x (x-a) P(a, b) db \\ &+ \operatorname{sgn}(x) \int_0^x (x-a) Q \left(a \operatorname{sgn}(x) \right) da \end{aligned}$$

$$\begin{aligned}
&= \sum_{i=1}^{N+1} \sum_{\substack{j=1 \\ i+j \text{ even}}}^{N+1} a_{ij} \left[\int_{-x_m}^x da \int_{x_o}^{x_m} (x-a) a^{i-1} b^{j-1} db \right. \\
&\quad \left. + \int_x^{x_o} da \int_{-x_m}^x (x-a) a^{i-1} b^{j-1} db \right] + \sum_{i=1}^{N+1} b_i \cdot B_i(x)
\end{aligned}$$

or

$$f'(x) = \sum_{i=1}^{N+1} \sum_{\substack{j=1 \\ i+j \text{ even}}}^{N+1} a_{ij} H_{ij}^I(x, x_o) + \sum_{i=1}^{N+1} b_i B_i(x)$$

where

$$\begin{aligned}
H_{ij}^I(x, x_o) &= \int_{-x_m}^x da \int_{x_o}^{x_m} (x-a) a^{i-1} b^{j-1} db \\
&\quad + \int_x^{x_o} da \int_{-x_m}^x (x-a) a^{i-1} b^{j-1} db
\end{aligned}$$

Note the role played by the "turn-around" value x_o . It is very suggestive of a state variable. The ramifications of this observation will be winnowed out in a later chapter.

Cyclically-Demagnetized Remagnetization Curve:

The planar region extant under cyclic demagnetization has already been depicted. If, after cyclic demagnetization, the input increases from zero monotonically past the saturation value, the CDRC will be generated. At any point x ,

$$\begin{aligned}
f'(x) &= \int_x^{x_m} db \int_{-b}^x (x-a) P(a, b) da + \int_{-x_m}^x db \int_x^{-b} (x-a) P(a, b) da \\
&\quad + \operatorname{sgn}(x) \int_0^x (x-a) Q(a \operatorname{sgn}(x)) da
\end{aligned}$$



$$\begin{aligned}
&= \sum_{i=1}^{N+1} \sum_{\substack{j=1 \\ i+j \text{ even}}}^{N+1} a_{ij} \left[\int_x^{x_m} db \int_{-b}^x (x-a) a^{i-1} b^{j-1} da \right. \\
&\quad \left. + \int_{-x_m}^x db \int_x^{-b} (x-a) a^{i-1} b^{j-1} da \right] + \sum_{i=1}^{N+1} b_i \cdot B_i(x)
\end{aligned}$$

or

$$f'(x) = \sum_{i=1}^{N+1} \sum_{\substack{j=1 \\ i+j \text{ even}}}^{N+1} a_{ij} H_{ij}'(x) + \sum_{i=1}^{N+1} b_i \cdot B_i(x)$$

where

$$\begin{aligned}
H_{ij}'(x) &= \int_x^{x_m} db \int_{-b}^x (x-a) a^{i-1} b^{j-1} da \\
&\quad + \int_{-x_m}^x db \int_x^{-b} (x-a) a^{i-1} b^{j-1} da
\end{aligned}$$

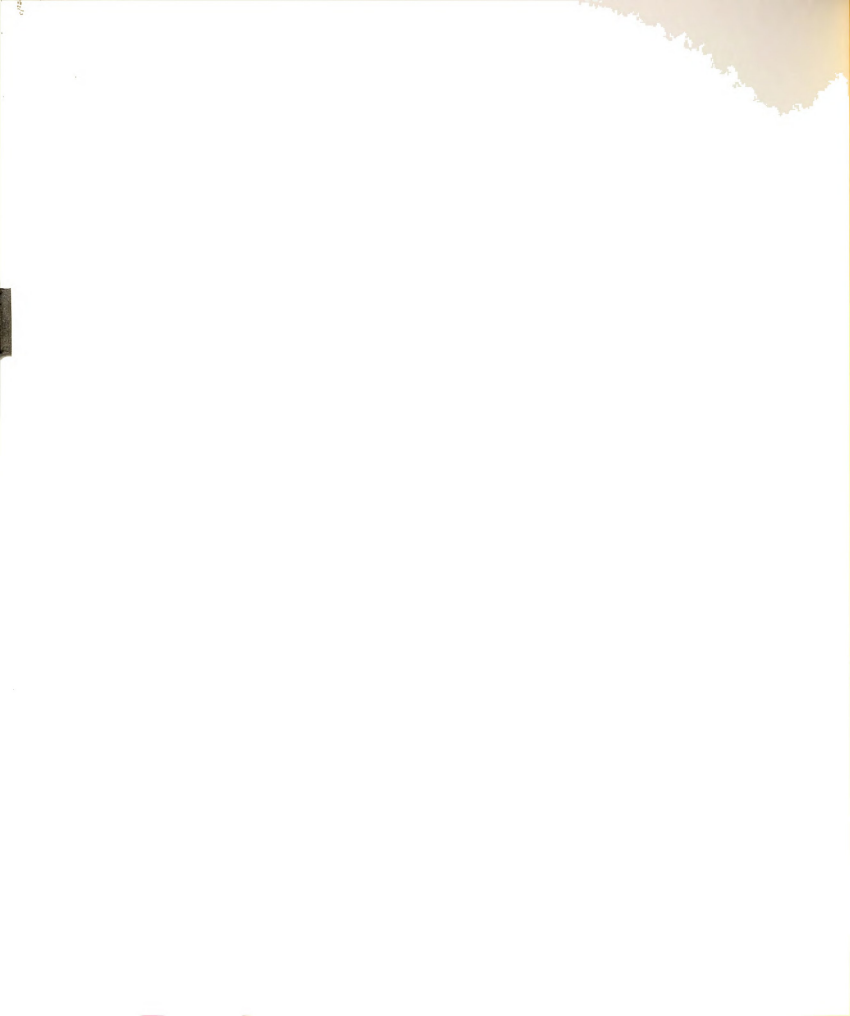
By generalization on the above results and some study of the configurations in the plane, it is apparent that the force after an arbitrary sequence of input variations can be written as an integral expression. Hence, a finite-sum approximation is available for any input. Another, and very important, feature should also be noted. Each of the above expressions for the force approximation is linear in the unknowns. The indices can be reordered such that each is a single dimensional linear combination of the unknowns, with the coefficients being the defined functions of x . An additional feature is the ease of calculation of these coefficients--the double integrations involve only powers and are easily computed on the machine.

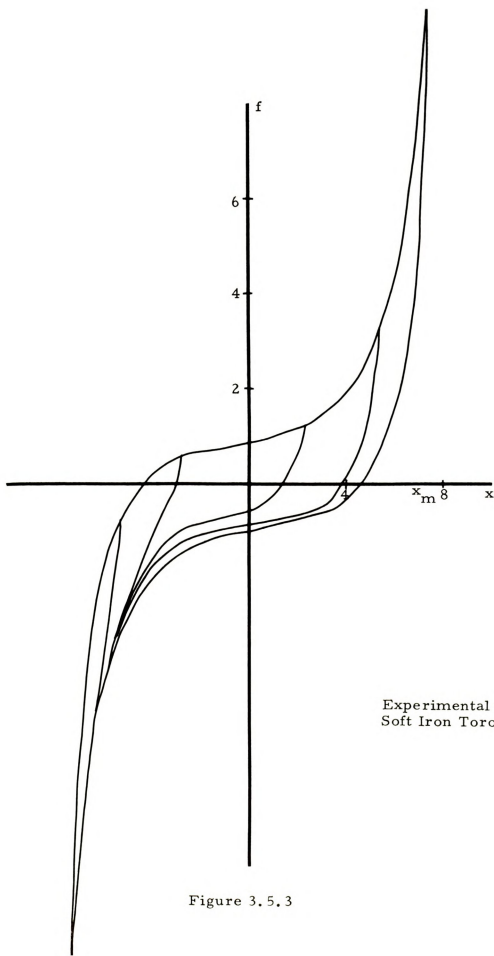
The linearity of the equations in the unknowns a_{ij} indicates the applicability of a linear least-squares technique. The particular one chosen is embodied in a routine available from the IBM Scientific

Subroutine Package. It utilizes Householder's²⁰ method for transforming an arbitrary matrix to triangular form through the application of unitary transformations. This procedure is attractive from a numerical standpoint.

Synthesis results are very nicely demonstrated by the accompanying figures. Some show relations obtained experimentally. Others are due to the synthesized model. Computed polynomial parameters have been inserted into a continuous simulation routine which is described elsewhere in this thesis. The demonstrated synthesis results form the output of this routine. As is clearly evident, the synthesis procedure provides a close match between model and real device. Note that the figures have different scales. It also appears that the semimajor loops alone provide as accurate a model as that provided by their combination with the CDRC.

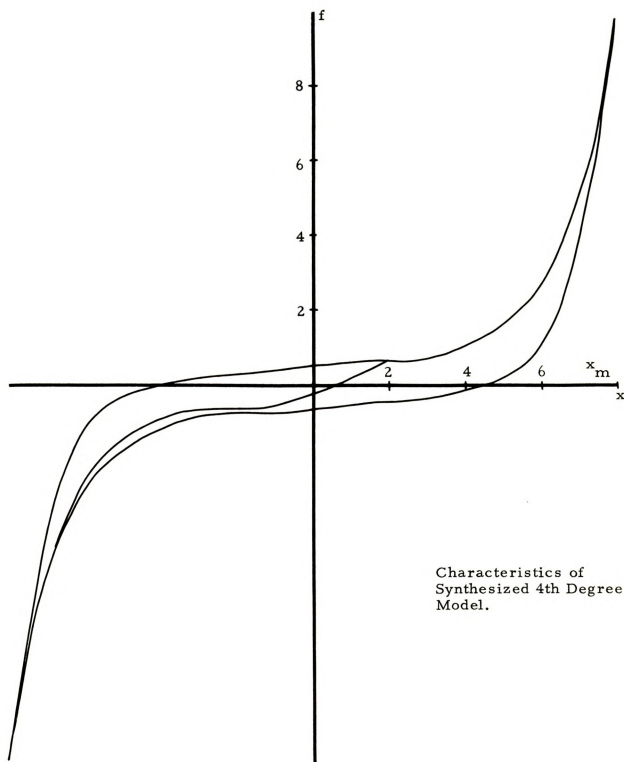
One of the attractive features of the polynomial approximation synthesis is its flexibility. If any additional type of behavior within the capabilities of the model is desired, it is relatively simple to incorporate such a fit into the existing procedure. For instance, if minor loops in a particular region are required to be represented more exactly, the desired equations can be included in the routine. Thus, at the expense of increase in complexity, it appears that a synthesis as accurate as desired can be obtained. The figures indicate the range of capability of the procedure. Materials of both soft and very hard composition, with their great variance in properties, have been successfully modeled.





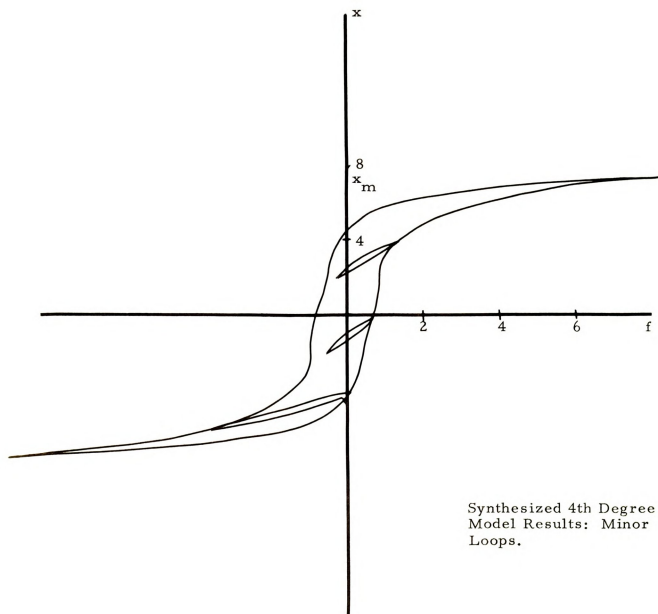
Experimental Data from
Soft Iron Toroid.

Figure 3.5.3



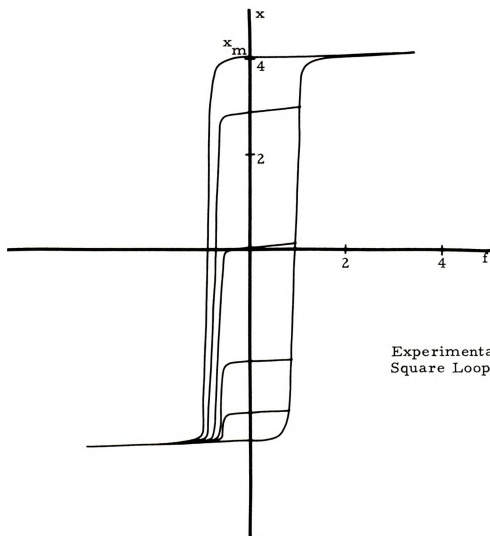
Characteristics of
Synthesized 4th Degree
Model.

Figure 3.5.4



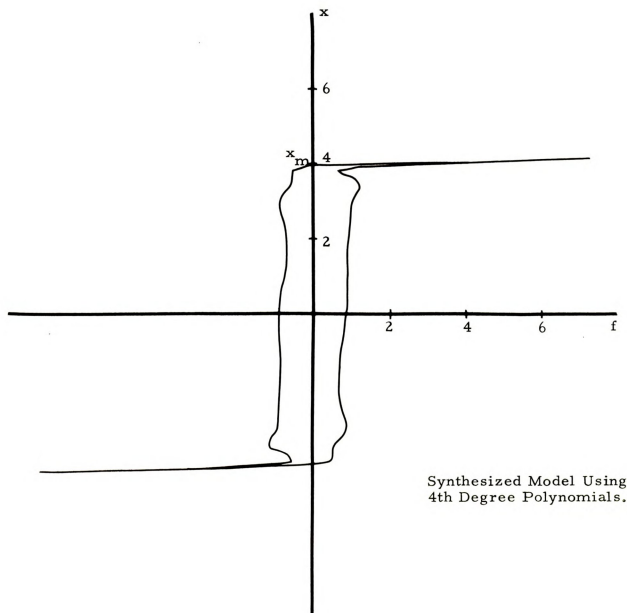
Synthesized 4th Degree
Model Results: Minor
Loops.

Figure 3.5.5



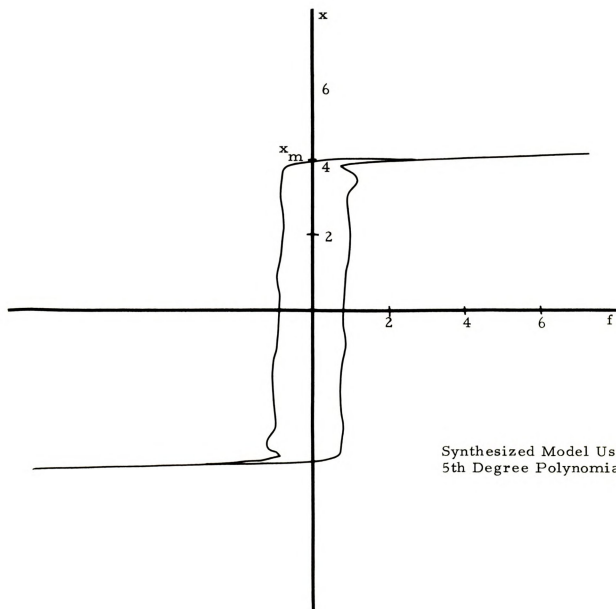
Experimental Data for
Square Loop Toroid.

Figure 3.5.6



Synthesized Model Using
4th Degree Polynomials.

Figure 3.5.7



Synthesized Model Using
5th Degree Polynomials.

Figure 3.5.8

CHAPTER IV

THE CONTINUOUS STATE MODEL

4.1. The Need for a Continuous Model

The early stages of this entire investigation hinged about the finite-beam discrete state model. As a tool, it was exceedingly useful at that point in time. It allowed an experimental program to be carried out that resulted in discovery of valuable first-order information about the model. As an efficient computational tool, though, it was found lacking. For each change in the input variable, the resulting value was subjected to a concatenation of several comparisons for each beam. Consequently, for a fairly large model--one involving perhaps hundreds of beams--the simulation was destined to be lengthy.

Another shortcoming of the discrete state model is its conceptual rigidity. Regardless of how many beams are incorporated into a model, the state space remains finite. On the other hand, the continuous analog admits a continuum of active-beam regions. Hence, it is essential that a more general state description be considered: one which will describe the continuous model as well as the discrete one.

4.2. The Continuous State Representation

As previously mentioned, it is possible to consider the continuous form of the beam-rod analogy as being the limiting case of

the finite-beam one. Unfortunately, this process does not yield a continuous state description; it is essential that the basic model features be re-examined in the plane. For ease of discussion, the term "beam" will be retained--it should be interpreted as meaning the discrete equivalent of a small planar region.

With an eye toward developing such a state model, consider the following possible active-beam pattern in the plane:

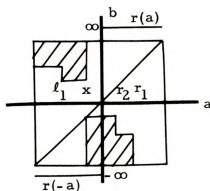


Figure 4.2.1

This pattern is a prototype of an entire class. There are two such classes, depending on the sign of the velocity of the rod, \dot{x} . The force resulting from the active-beam region is obtainable by analogy with the discrete model:

$$f(x) = \iint_Q (x - a) \phi(a, b) da db + g(x)$$

where $Q = Q^+ \cup Q^-$ is the region of active beams, and $g(x)$ is an input-determined function given by

$$g(x) = \begin{cases} \int_0^x (x - a) r(a) da; & x \geq 0 \\ \int_x^0 (x - a) r(-a) da; & x < 0 \end{cases}$$

or

$$g(x) = \operatorname{sgn}(x) \int_0^x (x-a) r(a \operatorname{sgn}(x)) da$$

It is possible then to loosely consider Q as the state of the model. Q is a function of the entire time function $x(\cdot)$ up to time t (the device is nonanticipative). It is also possible to write the above expression in the form

$$f(x) = \iint (x-a) S(a,b) \phi(a,b) da db + g(x)$$

where $S(a,b)$ is the characteristic function of the set Q ,

$$S(a,b) = \begin{cases} 1, & (a,b) \in Q \\ 0, & (a,b) \notin Q \end{cases}$$

and the integral is taken over the entire plane, or equivalently over the support of ϕ . Either of the above equations qualifies as an input-output state relation. In order that the state description be complete, it is essential that a method be available for describing state transitions as a function of the input. It is also necessary to make the definition of the state of the model a little more concrete. Such a state description is available, but before it can be developed, it is essential that the characteristics of the active regions be elaborated upon.

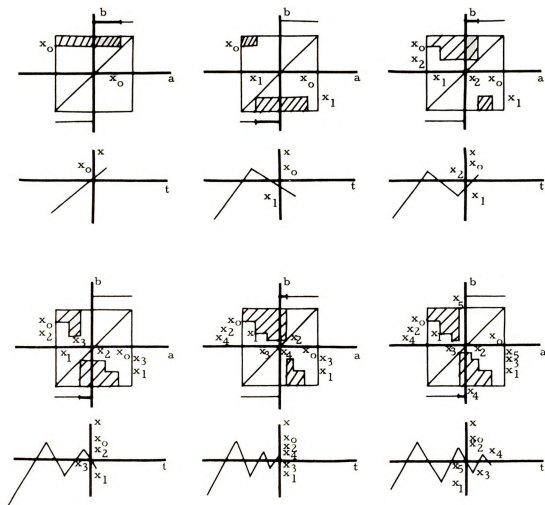
One of the most striking features of the region Q is its non-connected nature. It can be described as the union of two regions, Q^+ and Q^- , where Q^+ is the region of engaged right-active beams, and Q^- is the region of engaged left-active beams. If $x < 0$ at the instant of validity of the description of the region, as in Figure 4.2.1, the top left corner of Q^- will fall on the $b = a$ line. If $x > 0$, the lower right corner of Q^+ will fall on this line. The regions Q^+ and Q^-

exhibit very regular features: in fact, they are horizontal- and vertical-edged polygons in the plane. As such, they are completely determined by their "convex corners"; i. e., those which protrude from the regions. The ensuing development will describe this representation, and will elaborate upon the state space of the model.

In order to fix ideas, assume that the region under discussion is Q^+ , the region of engaged right-active beams. The properties of Q^- are exactly analogous to those of Q^+ . The upper boundary of Q^+ is a line segment with right endpoint at (x, x_m) . The left and right boundaries are vertical line segments whose endpoints will shortly be described.

Perhaps the most lucid description of the region Q^+ is a sequential account of the manner in which it takes form under a prototypic input waveform. A representative sequence of events is sketched in Figure 4.2.2. There are several important features of note. The convex edges, other than perhaps the sidecorners, reside at points in the plane given by (ℓ_i, r_i) , where $\{\ell_i\}$ is the sequence of points within the interval $(-x_m, x_m)$ where $x(t)$ "turns around" from left to right; that is, where $x(t)$ changes from monotone decreasing to monotone increasing. $\{r_i\}$ is the sequence of right "turn-around" points. The bottom left-most corner is given by $(-x_m, r_1)$ if the first turn-around was on the right, and by (ℓ_1, r_1) if the first turn-around was on the left. The bottom right-most corner is given by (x, r_{last}) , where r_{last} is the last turn-around on the right if x is decreasing, and by (x, x) if x is increasing.

The principle result of such a description of the active beam regions is an analytical definition of the state of the model--it is



Formation of Active Beam
Pattern Under a Prototypic
Input.

Figure 4.2.2

difficult to manipulate patterns. The two sequences $\{t_i\}$ and $\{r_i\}$ above can be combined into one; namely, $\{x_i\}$, the set of turn-around points of $x(t)$. One other item must be available, as mentioned above, for a viable state description. This quantity is the sign of the derivative of x , $\text{sgn}(\dot{x}(t))$. An alternative is to keep record of the nature of the last turn-around; that is, whether it was of the left or right kind. Hence, an element of the state space of the model is given by the pair (v, \bar{x}) , where $v = \text{sgn}(\dot{x})$, and $\bar{x} = \{x_i\}$, the turn-around sequence.

Now that the nature of the state space is clear, the only task remaining is the derivation of an algorithm for finding the state for any input function segment, given any initial state. Note that the state must yield to some rather obvious restrictions: there cannot be two successive turn-arounds of the same kind, and so forth. Suppose then that an initial state is given. This means specifically that the sign of the velocity at some time t_0 is given, as well as the last left and right turn-arounds. Then, a little contemplation of such a diagram as Figure 4.2.2 indicates the following:

1. If $x(t)$ exceeds either the last left or the last right turn-around, both are deleted from the sequence \bar{x} . The sequence is then reindexed so that the previous next-to-last pair is now the last pair (in indicial terms).
2. If $\dot{x}(t)$ changes sign at some time t' , without having committed an excess as described in part one, $x(t')$ is appropriately assigned as the new last element after the sequence is reindexed.

3. If $x(t)$ exceeds either $+x_m$ or $-x_m$, the sequence becomes vacuous, and the model is input-determined.

Although a state transition function is not available in closed form, the above discussion provides a basis for a practical state transition algorithm. Its implementation will be considered in the next section.

4.3. The Continuous Simulation Algorithm

Once the nature of the state space has been brought to light, it is important to consider its practical usage. The most pressing need is for a simulation routine which will accept the model parameters and deliver, for an arbitrary input, the output time function. This is important, both as a tool for checking the validity of a synthesized model and as an adjunct to other routines in a general network simulation package.

In the digital machine, the time variable ranges over a discrete set; this implies a somewhat simpler method for finding turn-around points. In the continuous time case, a turn-around point is a value x_i such that $x(t) = x_i$, $\dot{x}(t) = 0$, and $\ddot{x}(t) \neq 0$ for some t . In the discrete time case, a turn-around point is a value x_i such that $x(t_k) = x_i$ for some value of k and either

$$1. \quad x(t_{k-1}) < x_i, \quad x(t_{k+1}) > x_i$$

or

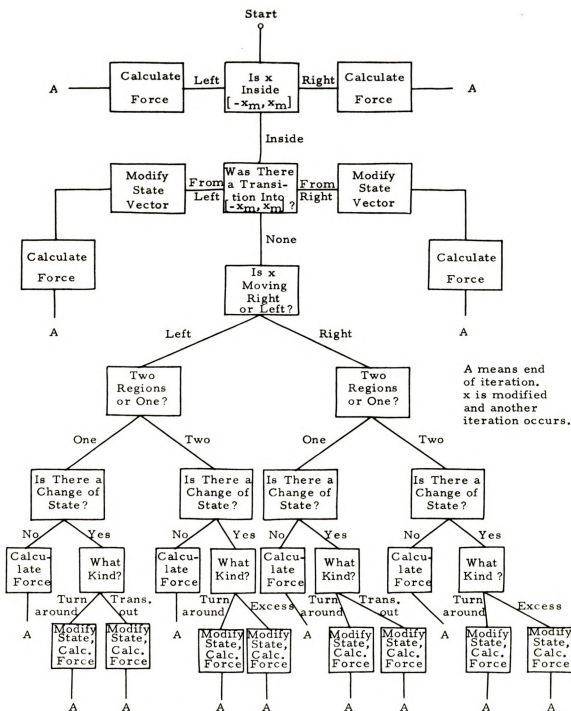
$$2. \quad x(t_{k-1}) > x_i, \quad x(t_{k+1}) < x_i$$

No derivatives need be calculated. The direction of motion of x is available by storing the character of the last turn-around point. If this is done, it is only necessary to compare the two most current points.

The procedure for modifying the state was outlined in the previous section, but there are some special cases. If the saturation loop is being traversed, there is only one active beam region. In this case, a turn-around indicates the inception of a new region. The theory still applies, but special care is required in its implementation. The fact that this can occur as a consequence of either of two types of turn-arounds compounds the complexity. These happenstances are provided for in a straight-forward fashion, but some care is required in the programming. The logical flow diagram for state transition determination in the simulation algorithm is presented in Figure 4.3.1. Other details of the algorithm are straight-forward.

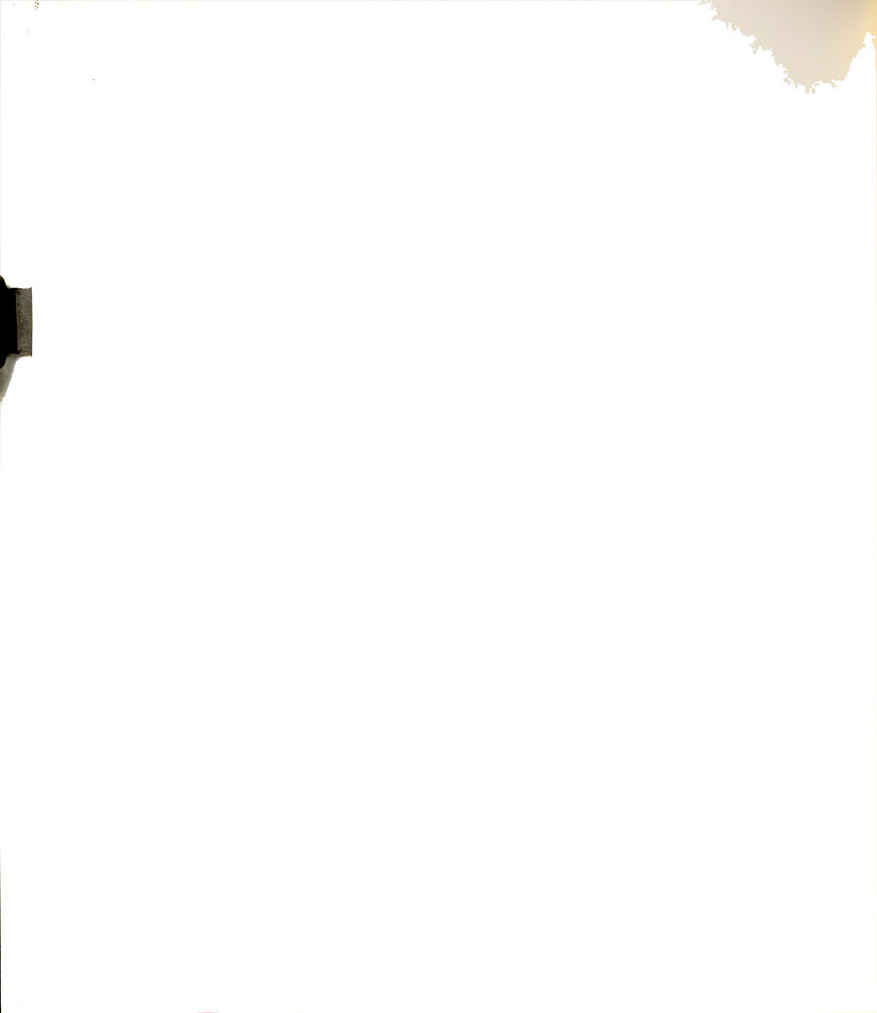
Once the state is found, the output can be evaluated by solving the input-output relation for a given instantaneous value of the input. If the model under consideration is discrete, this involves the evaluation of a finite sum; if the model is continuous, a double integral must be evaluated. This is the only modification required when changing the algorithm to accept one or the other--the state transition algorithm remains the same. In the evaluation of the input-output state relation (in either case), two techniques can be used: the integral or sum can be taken over the entire active region at each iteration, or it can be calculated only over the regions of newly acquired and recently dropped beams. In the latter case, the process is more susceptible to accumulation of error. The former case is better from a numerical point of view, but is slower.

The differential type of algorithm was selected for implementation because of its speed. Figure 4.3.2 shows the nature of a typical



State Transition Logic for Continuous Algorithm

Figure 4.3.1

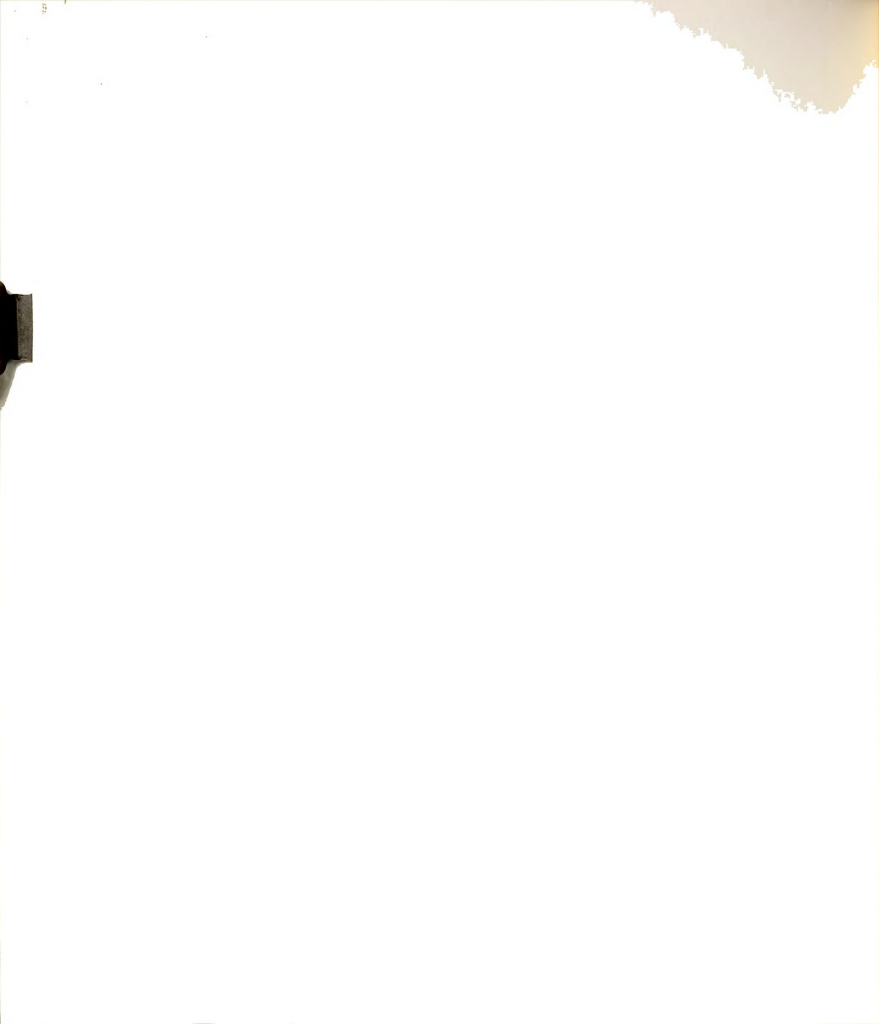


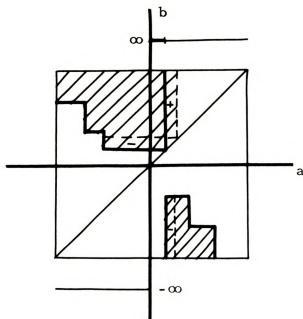
change in the active beam region. Utilizing the discrete model for comparison with the discrete algorithm, the continuous version proved to be on the order of six to ten times faster for typical inputs. No problem was encountered with error accumulation. The blackboard of past history is erased when operation enters the saturation region; but for long-duration inputs which do not drive the device into saturation, error accumulation could become significant.

The algorithm presented above is complete; that is, given the initial state and future values of the input, the future output can be determined. For the studies being described in this thesis, however, it was not essential that the initial state be provided. All inputs utilized possessed the happy feature of starting in one of the saturation regions. In this region, the model is input determined, so no initial state was required. As soon as the operation enters the non-saturation zone, the algorithm commences to generate its own states. Hence, the flow diagram of Figure 4.3.1 does not provide for inserting an initial state.

One item of interest pertaining to operation of the algorithm is the fact that, theoretically, the sequence associated with the state can be of infinite extent. In view of the fact that machine storage is finite, something must be known about the nature of the input waveform so that storage bounds can be set. In the absence of such knowledge, a reasonable amount of storage can be allocated, and a monitor can be set up to warn of imminent overflow.

It is possible to summarize the advantages of the continuous algorithm by reiterating the fact that it subsumes the discrete model and allows for greater generality, both computationally and



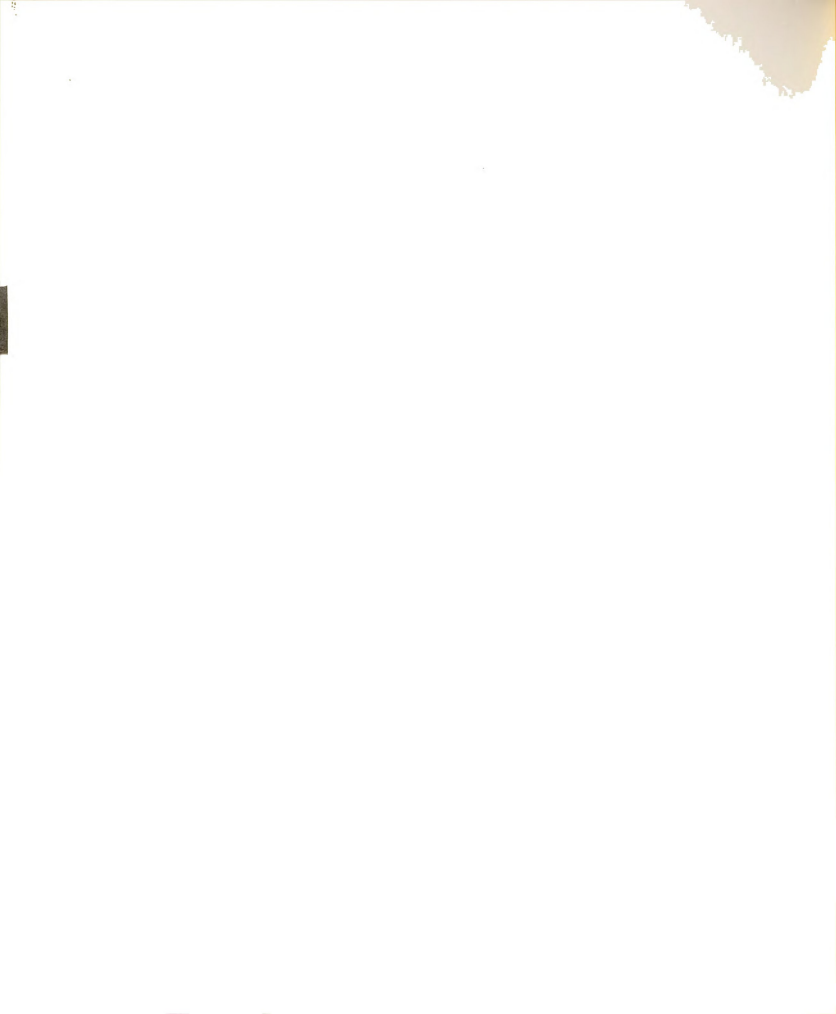


+: beams acquired

-: beams dropped

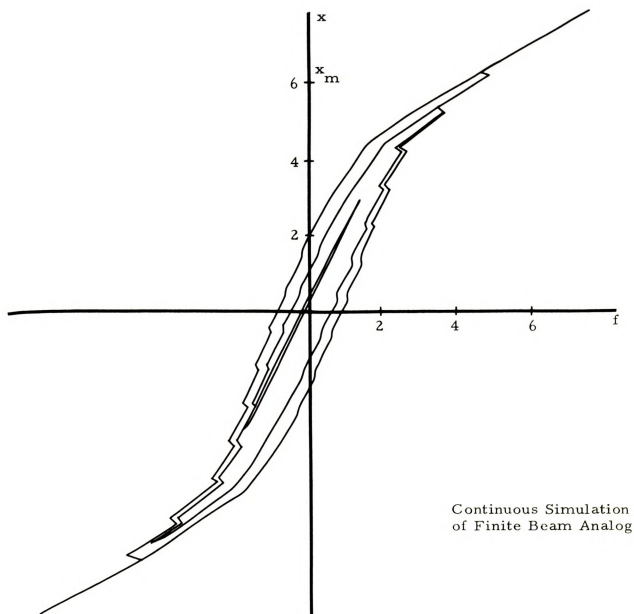
Change of Active Beam Region

Figure 4.3.2



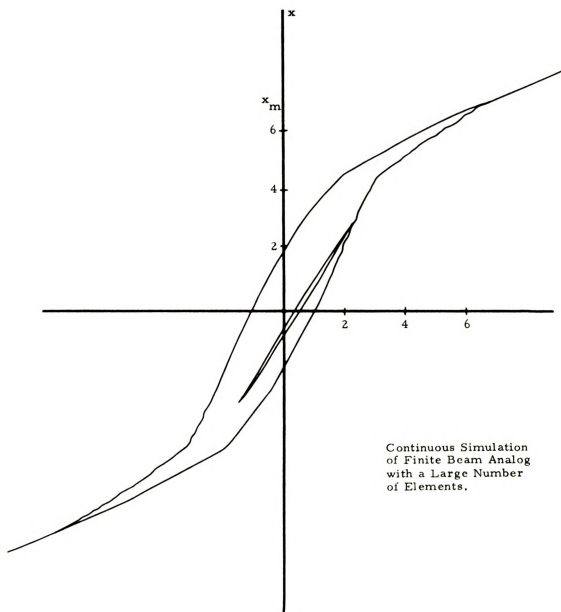
conceptually. Several model characteristics are plotted in Figures 4.3.3 and the following two in order that those assertions be substantiated by graphical evidence.

Handwritten text, possibly a date or page number, located in the top right corner.



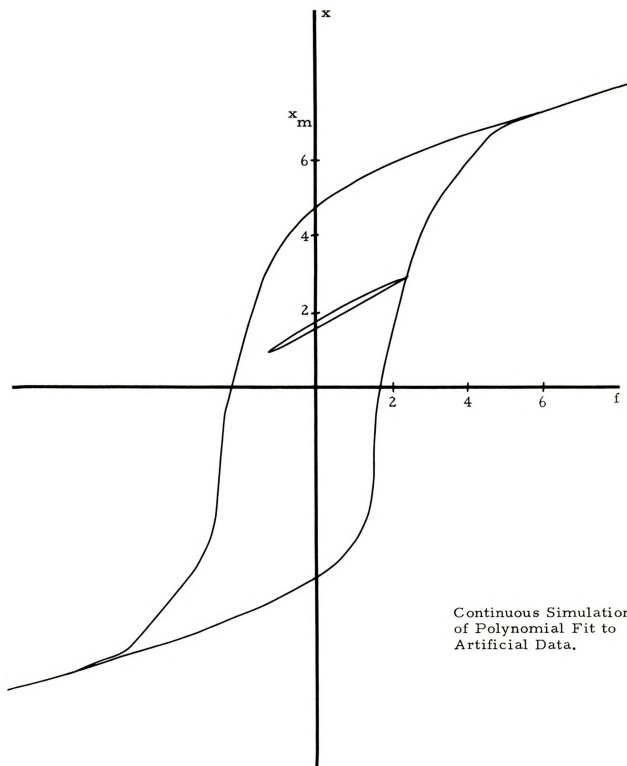
Continuous Simulation
of Finite Beam Analog

Figure 4.3.3



Continuous Simulation
of Finite Beam Analog
with a Large Number
of Elements.

Figure 4.3.4



Continuous Simulation
of Polynomial Fit to
Artificial Data.

Figure 4. 3. 5

CHAPTER V

CONCLUSIONS

In the course of the investigation described in these pages, a number of important advances were made. Beginning with Resh's basic model and continuing through the development of a rather complex, but efficient, simulation algorithm, a continuing path of progress was traversed. That path has not halted in a cul-de-sac, but has branched out into a multiplicity of paths. Several seem to beckon with the promise of dramatic developments ahead.

The view back along the path reveals the following concrete results. A discrete state model was developed for the original finite beam analog. It was used to more fully explore the capabilities of that model, as well as to derive the support of the characterizing beam elasticity density function. A continuous analog was derived by proceeding from the finite-beam version. A synthesis algorithm was developed for the continuous model, and a set of experimental measurements was developed to support that procedure. Finally, a continuous state algorithm was developed which provides a fast, efficient simulation of either the discrete or the continuous analog.

The mainstream of the work embodied here flowed along three channels: theoretical, laboratory experimental, and computer simulation experimental. Transition was made frequently from one area to another in order to bulwark an idea conceived in one with results from another.

As a result of the work done here, it is possible to experimentally characterize iron core inductors with either hard or soft cores; to synthesize the model parameters; and, utilizing the continuous state algorithm, to incorporate these inductors into a larger network for simulation purposes. The techniques developed here are also directly applicable to the most important of the earlier models, that of Preisach.

At the present stage of development, it is possible to glimpse a few outlines of developments along the paths ahead. As work has progressed, an intuitive idea has been taking form of the general nature of the distribution function ϕ . It should be non-negative definite and should peak near the $b = a$ line. It will perhaps be possible to utilize this characteristic to advantage.

Another intuitive idea is the following: Magnetic dipoles, gas molecules, and the like, are distributed in number exponentially with energy. The function $\phi(a, b)$ can be considered as that density function such that $\phi(a, b) da db$ is the number of beams of unit elasticity coefficient in the elemental area $da db$. The maximum energy stored in one such beam is given by $\frac{1}{2}(b - a)^2$. Hence, it is reasonable to assume that

$$\phi(a, b) = K e^{-\left(\frac{b-a}{\sigma}\right)^2}$$

where σ is a dispersion factor and K is a constant. Indeed, promising results have already been obtained for this assumed form.

A large amount of effort has gone into attempting the synthesis of the discrete analog. All efforts have ultimately failed, although valuable insight has resulted from each attempt. The basic problem lies in determining an independent set of measurements. In almost

all cases, a set of K measurements resulted in a set of $K-1$ independent equations. It seems that not enough is known about the relation between sets of physical measurements and the dependence characteristics of the resulting set of mathematical equations. Another exacerbating factor pertaining to synthesis of the discrete model is its complexity. Even if the resulting equations were independent, the system order is high. This would perhaps require sparse matrix techniques, and it would certainly entail a closer investigation of the spreading technique mentioned in the text. Of course, least squares synthesis is also plausible in the discrete case.

Another area for future work pertains to the goodness of fit qualities of the continuous synthesis procedure. What should be the distribution of measured data in order to provide the best fit? What should be the relative orders of the boundary and body polynomials to provide the best fit with accompanying reasonable computing time?

Finally, there is the question of frequency effects. Can these rate dependent facets of hysteresis be accounted for by the finite mass beam-rod interaction dynamics of the analog? It appears reasonable to tackle this problem through the means of "fuzzy" set theory, for example. In any event, this particular avenue of development has, as yet, remained untraveled.

Thus, in addition to the concrete results which have been established, it appears that prospects are bright for future extensions to the current work.

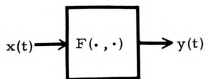
REFERENCES

1. Attinger, E. O., "Wall Properties of Veins," IEEE Trans. on Biomedical Engineering, BME-16, No. 4, pp. 253-261 (1969).
2. Volterra, E., "Vibrations of Elastic Systems Having Hereditary Characteristics," J. of Applied Mechanics, Vol. 17, No. 4, pp. 363-371, December, 1950.
3. Brown, D. A. H., "Behavior of Square Loop Magnetic Cores in Circuits," Electronic Engineering, Vol. 31, No. 377, pp. 408-412, July 1959.
4. Topp, G. C., "Soil-Water Hysteresis: The Domain Theory Extended to Pore Interaction Conditions," Soil Science Society of America Proceedings, Vol. 35, No. 2, p. 219, March-April, 1971.
5. Resh, J. A., "Towards General Simulation of Ferromagnetic Devices," Proc. 1969 12th Midwest Symposium on Circuit Theory, pp. V.2.1-V.2.7, April, 1969.
6. Ewing, J. A., Magnetic Induction in Iron and Other Metals, The Electrician Publishing Company, London, p. 294, 1900.
7. Bitter, Francis, Introduction to Ferromagnetism, McGraw-Hill, New York, 1937.
8. Darrow, Karl K., "Contemporary Advances in Physics--XIII, Ferromagnetism," Bell System Technical Journal, Vol. 6, p. 295, April, 1927.
9. Weiss, P. and J. DeFreundenreich, Arch. Sc. Nat. (Geneva), Vol. 42, p. 449, 1916.
10. Langevin, P., Ann. Chim. Phys., Vol. 5, No. 8, p. 70, 1905.
11. Volterra, V., Theory of Functionals and of Integral and Integro-Differential Equations, Dover, New York, 1959.
12. Preisach, F., "Über die Magnetische Nachwirkung," Z. Physik, Vol. 94, p. 277, 1935.
13. Biorci, G. and D. Pescetti, "Analytical Theory of the Behavior of Ferromagnetic Materials," Nuovo Cimento, Vol. 7, No. 6, p. 829, 1958.

14. Chua, L. O. and K. Stromsmoe, "Synthesis of Lumped Circuit Models for Nonlinear Inductors Exhibiting Hysteresis Loops," Purdue University School of Electrical Engineering Technical Report, TR-EE69-20, June, 1969.
15. Iwan, W. D., "A Distributed-Element Model for Hysteresis and its Steady-State Dynamic Response," J. of Applied Mechanics, Vol. 33, No. 4, p. 893, December, 1966.
16. McKeehan, L. W., Magnets, Van Nostrand, Princeton, 1967.
17. Cioffi, P., "A Recording Fluxmeter of High Accuracy and Sensitivity," Review of Scientific Instruments, Vol. 21, No. 7, July, 1950.
18. Berge and Guderjahn, "Recording Fluxmeter," Electronics, Vol. 27, No. 7, p. 147, July, 1954.
19. Bockemuehl and Sargent, "Practical Hysteresigraph," Journal of Applied Physics, p. 180s, May, 1960.
20. Householder, A. S., "Unitary Triangularization of a Nonsymmetric Matrix," J. of the Assoc. for Computing Mach., Vol. 5, p. 339, 1958.

APPENDIX THE PRACTICAL ASPECTS OF INTEGRATION

An ideal integrator, mathematically perfect, can be represented by:



where the operator F is defined by

$$F(x, t) = \int_0^t x(a) da \quad \forall t \geq 0$$

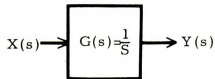
The LaPlace transform of the output time function $y(t)$ is related to that of the input by

$$Y(s) = \frac{1}{s} (X(s) + y(0))$$

or assuming $y(0) = 0$,

$$Y(s) = \frac{1}{s} X(s)$$

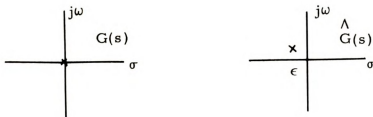
The integrator can thus be represented by a transfer function $G(s) = 1/s$,



Now consider the practical aspect of realizing $G(s)$. This is impossible to perform exactly, for the pole at the s -plane origin represents

an infinite dc gain. This fact implies that any attempt to integrate a variable will face practical obstacles.

The obvious, and probably the best (in some sense) approximation to $G(s)$ is by a transfer function which consists of a simple pole perturbed from the origin by a slight amount.



Then,

$$\hat{G}(s) = \frac{1}{s - \epsilon}$$

Now ϵ cannot be perfectly arbitrary, for the dc gain is now $-\frac{1}{\epsilon}$, and it must be real if \hat{G} is to be realizable. The case where $\epsilon > 0$ is also ruled out because this would imply instability. Hence, $\hat{G}(s)$ can practically be approximated by the above $\hat{G}(s)$ for $\epsilon < 0$, and the approximation converges to the ideal form as $\epsilon \rightarrow 0^-$.

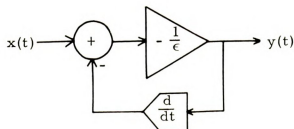
Reverting to the time domain, the transform version of the input-output relation

$$(s - \epsilon)Y(s) = X(s)$$

becomes

$$\frac{dy}{dt} - \epsilon y = x(t)$$

Thus, the imperfect integrator can be modeled by:



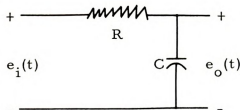
It is found that in practice virtually all integrator circuits can be modeled by the above abstract form, or by the differential equation

$$\frac{dy}{dt} + \mu y = x$$

Note that $\mu = -\epsilon = \frac{1}{A}$, where A is the amplifier gain.

The generality of this abstract integrator model can easily be seen by consideration of a number of examples. It should be observed that such examples tend to fall into two categories: those whose imperfection is due to imperfect elements and those which contain ideal elements, but are imperfect for structural reasons. The addition of imperfect elements to the latter category merely exacerbate the situation.

Example 1:



This circuit is an old friend, almost a party regular, because of its simplicity and passive elements. Summing currents at the output node results in

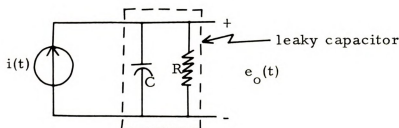
$$\frac{e_i - e_o}{R} - C \frac{de_o}{dt} = 0$$

or

$$\frac{de_o}{dt} + \frac{1}{RC} e_o = \frac{1}{RC} e_i$$

If the substitutions $y = e_o$ and $e_i/RC = x$ are made, it is evident that the governing relation is of the form $\frac{dy}{dt} + \mu y = x$ with $\mu = \frac{1}{RC}$. This circuit falls into the second category, for it is imperfect even though the components are assumed ideal. A further disadvantage stems from the fact that as $\mu \rightarrow 0$, $x \rightarrow 0$. Thus, even though the amplifier gain in the abstract model is increasing, the attenuation in the actual circuit is going up.

Example 2:



In this circuit, if the capacitor were ideal, the integration would be perfect, for the terminal relation for a capacitor is $e(t) = \frac{1}{C} \int_0^t i(a) da + e(0)$. With this configuration, though, the capacitor is "leaky". Summing currents,

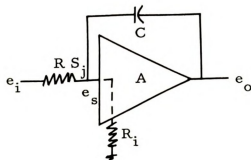
$$i(t) = C \frac{de_o}{dt} + \frac{e_o}{R}$$

or

$$\frac{de_o}{dt} + \frac{1}{RC} e_o = \frac{1}{C} i$$

which is in the general form with, once again, $\mu = \frac{1}{RC}$. As $R \rightarrow \infty$, $\mu \rightarrow 0$ and the capacitor becomes ideal. In this case, $x = \frac{i}{C}$, and no input attenuation results as $\mu \rightarrow 0$.



Example 3:

As a final example, consider the operational amplifier integrator with finite input impedance. Since the interest here is in very low frequency inputs, this is adequate allowance for non-ideal characteristics. Then, summing currents at S_i ,

$$\frac{e_i - e_s}{R} + C \frac{d}{dt} (e_o - e_s) = \frac{e_s}{R_i}$$

But, $e_s = e_o/A$, so

$$\frac{e_i}{R} - \left(\frac{1}{R} + \frac{1}{R_i} \right) \cdot \frac{1}{A} e_o + C \left(1 - \frac{1}{A} \right) \frac{de_o}{dt} = 0$$

or

$$\frac{de_o}{dt} - \frac{1}{(A-1)C} \cdot \left(\frac{1}{R} + \frac{1}{R_i} \right) e_o = -\frac{e_i}{R}$$

Hence, the general equation is once more satisfied with:

$$y = e_o, \quad x = -\frac{e_i}{R}, \quad \mu = -\frac{R + R_i}{(A-1)R R_i C}$$

A is ordinarily negative, and as $A \rightarrow -\infty$, $\mu \rightarrow 0^+$. There is no increase in attenuation. Since operational amplifiers are readily available with extremely high gains, this configuration is very attractive. Note, however, that it is of the second category, because if A is finite, $\mu \neq 0$ even though $R_i \rightarrow \infty$.



Analysis of Error:

Consideration of the general imperfect integrator equation

$$\frac{dy}{dt} + \mu y = x$$

once again yields the solution

$$y(t) = \int_0^t e^{-\mu(t-a)} x(a) da$$

where the initial value of y is assumed to be zero. The departure from ideal is given by the multiplicative factor $e^{-\mu(t-a)}$. If μ is very small, this term will be close to unity over the range of integration--if t is not too large. It is apparent that μ is a direct measure of the quality of the integrator.

Now, suppose the above equation is integrated by parts. There results:

$$y(t) = \int_0^t x(\sigma) d\sigma - \int_0^t \left[\int_0^a x(\sigma) d\sigma \right] \cdot \mu e^{-\mu(t-a)} da$$

Hence, the error after the passage of t units of time is:

$$\delta(t) = -\mu \int_0^t \left[\int_0^a x(\sigma) d\sigma \right] e^{-\mu(t-a)} da$$

and

$$y(t) = \int_0^t x(\sigma) d\sigma + \delta(t)$$

Suppose $x(t)$ changes and then remains at zero; that is, assume $x(t) \equiv 0$ for $t > T$. Then, for $t > T$,

$$y(t) = \int_0^T x(\sigma) d\sigma + \delta(t)$$

with

$$\delta(t) = e^{-\mu(t-T)} \cdot \delta(T) - [1 - e^{-\mu(t-T)}] \cdot \int_0^T x(\sigma) d\sigma$$



Thus,

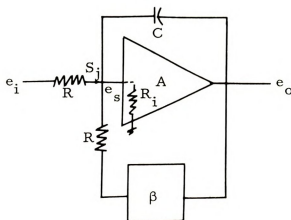
$$y(t) = e^{-\mu(t-T)} \left[\delta(T) + \int_0^T x(\sigma) d\sigma \right]$$

Hence, the output can be written

$$y(t) = y(T) e^{-\mu(t-T)}; \quad t \geq T$$

This represents a decaying exponential with time constant μ . Therefore, the decay time is a directly measurable criterion of integrator quality.

The fact that the decay time is inversely proportional to μ gives a clue to possible methods for improvement. The following one can be applied to any of the three previous examples, but the following discussion will center on the "op-amp".



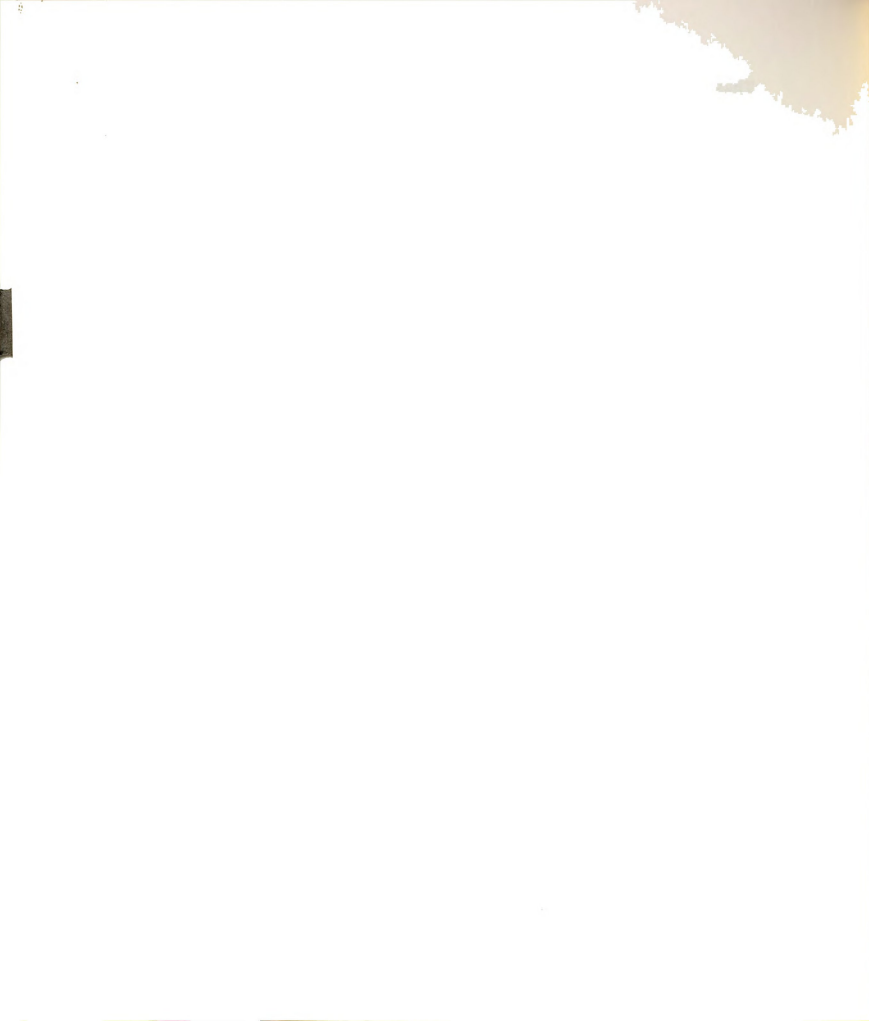
$$\frac{e_i - e_s}{R} + \frac{\beta e_o - e_s}{R} + C \frac{d}{dt} (e_o - e_s) = \frac{e_s}{R_i}$$

but, $e_s = e_o/A$, so

$$C(1 - A) \frac{de_o}{dt} + \left(\frac{\beta}{R} - \frac{2/A}{R} - \frac{1/A}{R_i} \right) e_o = -\frac{e_i}{R}$$

infinite decay time will result when the coefficient of e_o vanishes:

$$\frac{\beta}{R} - \frac{1}{A} \left(\frac{2}{R} + \frac{1}{R_i} \right) = 0$$



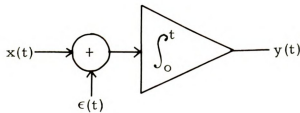
or

$$\beta = \frac{1}{A} \left(2 + \frac{R}{R_1} \right)$$

Consideration of the loop gain reveals that this is precisely the condition for oscillation. Hence, β must be adjusted for a magnitude somewhat below this figure. This same type of positive feedback can be applied to the other examples investigated. It has been applied quite successfully in the development of the ballistic galvanometer instruments mentioned in the text. These devices also fit the general model presented here.

Drift:

In spite of its other attractive features, the operational amplifier suffers from the bane of dc drift (a problem not so troublesome with the ballistic galvanometer instruments). This arises as a result of power supply voltage variation and the temperature dependence of transistor leakage currents. The resulting drift voltage at the output can be divided by the gain and referred to the amplifier input. Assuming that the op-amp is used in the configuration of Example 3, and that the overall integrator can be approximated otherwise as ideal (that is, $\mu = 0$)



Then,

$$y(t) = \int_0^t x(a) da + \int_0^t \epsilon(a) da$$

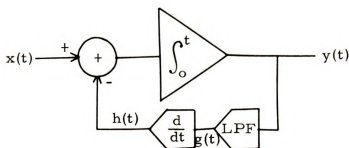


If ϵ is constant, for example,

$$y(t) = \int_0^t x(a) da + \epsilon \cdot t$$

Methods of Controlling Drift:

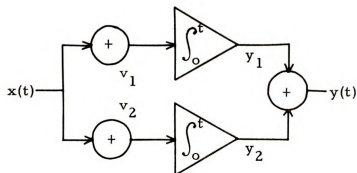
In some applications, the signal to be integrated does not contain frequency components extending to dc. For example, if a ferromagnet is excited by a sixty hertz mmf, the response voltage in a Faraday search coil has a fundamental of sixty hertz. In this case, the following scheme is effective:



Thus, since the integral of a slowly varying quantity is even more slowly varying, $g(t) = \int_0^t \epsilon(a) da$ and $h(t) = \epsilon(t)$. Thus, the drift has been eliminated.

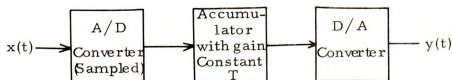
Other applications do not exhibit such nice features. If the input has frequency components extending to dc, another approach must be taken. Chopper stabilization is such an approach, and is well covered in the literature. Even with chopper stabilization, though, the drift is objectional when the signal to be integrated has very low amplitude. Further improvement can be effected by introducing a small compensating voltage at the summing junction--one which approximates the internal offset. An even further reduction can be made by using two integrators.



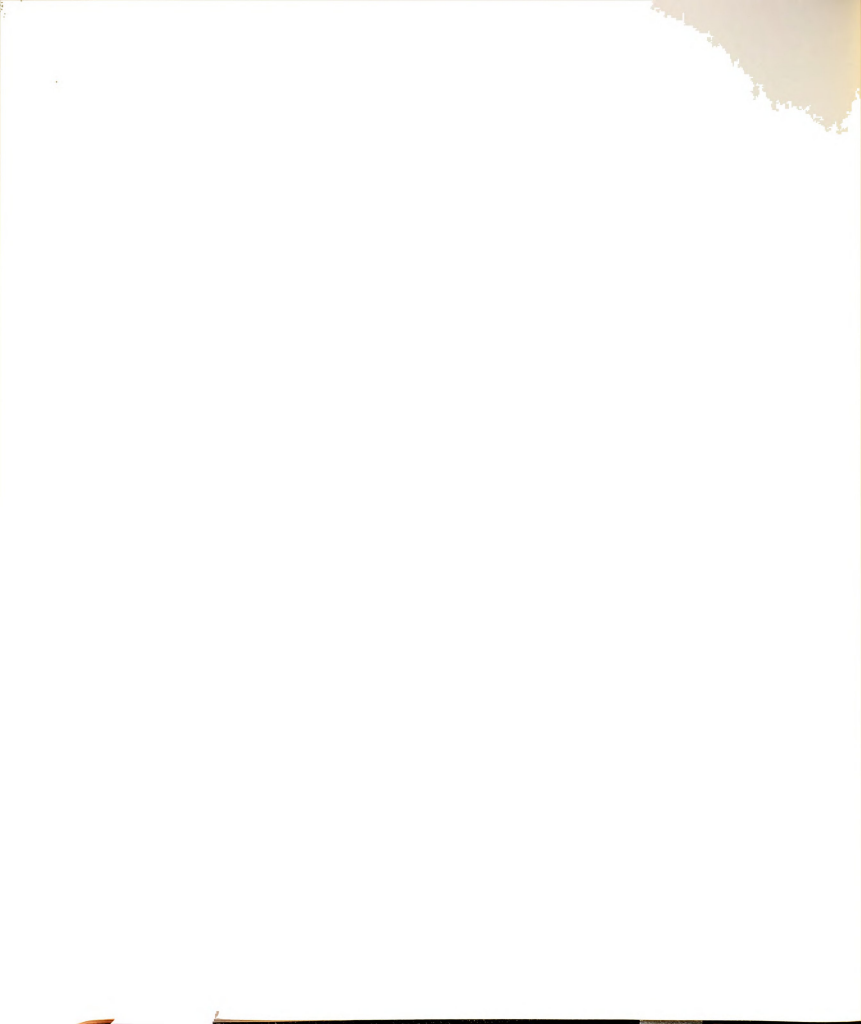


Operation is based on the following fact: Regardless of how fine one trims a compensation voltage, there is an average drift in one direction. Thus, the above circuit is adjusted such that "on the average" ϵ_1 is increasing and ϵ_2 decreasing, or vice versa. With $x(t) \equiv 0$, v_1 and v_2 are trimmed until the output is approximately zero for every t . In practice, this seems to provide good results. The two integrator amplifiers are physically mounted in propinquity to one another, so it is possible to match offsets rather closely.

The aforementioned technique is the one selected for the experimental work embodied in this thesis. Another possibility is at hand, though, and should be mentioned: the possibility of using digital integration techniques.

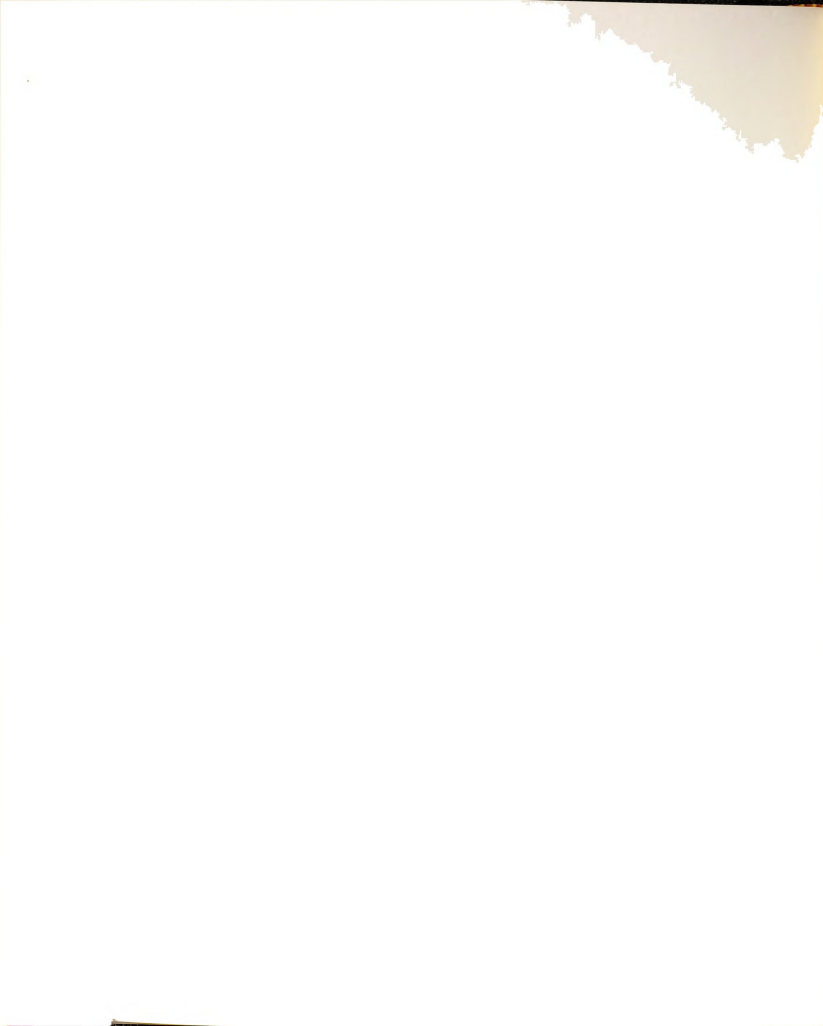


This setup essentially performs a Riemann Sum approximation to the integral. If T is the sampling period,



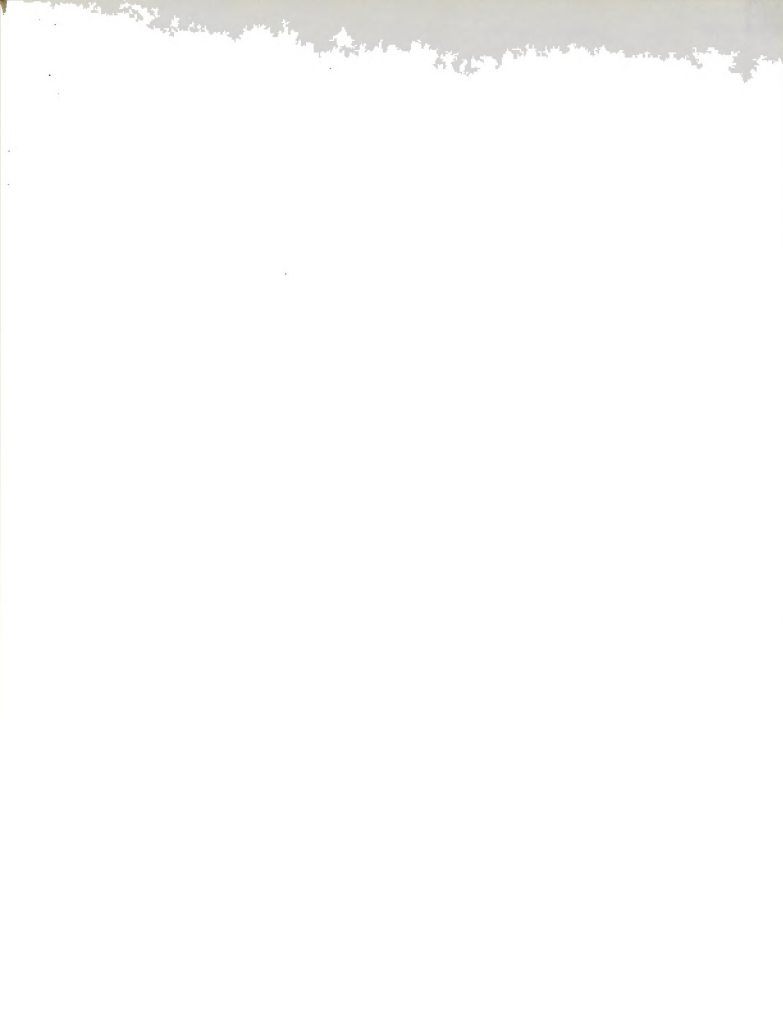
$$y(t) = \sum_{i=1}^{\lceil \frac{t}{T} \rceil} x(iT) \cdot T$$

where $\lceil \frac{t}{T} \rceil$ is the greatest integer function. As $T \rightarrow 0$, the above sum converges to the integral of x over $[0, T]$. Any offset in the A/D converter will show up in a fashion analogous to that for the analog integrator. Static offset, though, can be compensated for by feeding in zero level and subtracting that digital number from all forthcoming samples. It would be difficult to analyze this configuration for its error, but one factor is clear: digital stores are not "leaky", so the equivalent μ would be infinite.









MICHIGAN STATE UNIVERSITY LIBRARIES



3 1293 03070 9152